Title: Robust IgM responses following vaccination are associated with prevention of *Mycobacterium tuberculosis* infection in macaques

Authors: Edward B. Irvine[1,2], Anthony O'Neil[1], Patricia A. Darrah[3], Sally Shin[1], Alok Choudhary[4], Wenjun Li[5], William Honnen[4], Smriti Mehra[6], Deepak Kaushal[7], Hannah Priyadarshini Gideon[8], JoAnne L. Flynn[8], Mario Roederer[3], Robert A. Seder[3], Abraham Pinter[4], Sarah Fortune[1,2†]*, and Galit Alter[1†]*

Affiliations:

[1] Ragon Institute of MGH, MIT and Harvard; Cambridge, MA, USA.

[2] Harvard T.H. Chan School of Public Health; Boston, MA, USA.

[3] Vaccine Research Center, National Institute of Allergy and Infectious Diseases (NIAID), National Institutes of Health; Bethesda, MD, USA.

[4] Public Health Research Institute, New Jersey Medical School, Rutgers, The State University of New Jersey; Newark, NJ, USA.

[5] Department of Medicine, University of Massachusetts Medical School; Worcester, MA, USA.

[6] Division of Microbiology, Tulane National Primate Research Center; Covington, Louisiana, USA.

[7] Southwest National Primate Research Center, Texas Biomedical Research Institute; San Antonio, TX 78245, USA.

[8] Department of Microbiology and Molecular Genetics and Center for Vaccine Research, University of Pittsburgh School of Medicine; Pittsburgh, PA, USA.

[†] These authors contributed equally to this work.

* Correspondence: sfortune@hsph.harvard.edu (S.M.F.) and GALTER@mgh.harvard.edu (G.A.)

Abstract: Development of an effective tuberculosis (TB) vaccine has suffered from an incomplete understanding of the correlates of protection against *Mycobacterium tuberculosis* (*Mtb*). However, recent work has shown that compared to standard intradermal Bacille Calmette-Guerin (BCG) vaccination, intravenous (IV) BCG vaccination provides nearly complete protection against TB in rhesus macaques. While studies have focused on cellular immunity in this setting, the antibody response elicited by IV BCG vaccination remains incompletely defined. Using an agnostic antibody profiling approach, here we show that IV BCG drives superior antibody responses in the plasma and the bronchoalveolar lavage fluid (BAL). While IV BCG immunization resulted in the expansion of a robust IgM, IgG, IgA, Fc-receptor binding antibodies, and antibody effector functions in the BAL, IgM titers were among the strongest markers of reduced bacterial burden in the plasma and BAL of BCG immunized animals. Moreover, IgM immunity was also enriched among animals receiving protective vaccination with an attenuated *Mtb* strain. Finally, a LAM-specific IgM monoclonal antibody reduced *Mtb* survival *in vitro*. Collectively, these data highlight the potential importance of IgM responses as a marker and as a functional mediator of protection against TB.

39 **Main Text:**

40 **INTRODUCTION**

41 *Mycobacterium tuberculosis* (*Mtb*), the causative agent of tuberculosis (TB), was responsible for
42 the death of an estimated 1.4 million individuals in 2019 (*1*). While TB is curable, the intensive antibiotic
43 regimen coupled with the rise in antibiotic resistance has underscored the need for an efficacious vaccine
44 to help mitigate the global TB epidemic. Bacille Calmette-Guérin (BCG), first introduced in 1921, is the
45 current standard for TB vaccination (*2*). While BCG is effective at preventing severe forms of TB in young
46 children, BCG is poorly and variably efficacious in preventing pulmonary TB in adults (*3*). Consequently,
47 novel vaccines and vaccination strategies are urgently needed.

48 TB vaccine development has suffered from a lack of understanding of the determinants of
49 immunity against *Mtb* infection. CD4+ T cell knock-out studies in mice (*4*, *5*), CD4+ depletion and simian
50 immunodeficiency virus infection studies in non-human primates (NHPs) (*6*–*8*), as well as human
51 immunodeficiency virus infected human cohort studies (*9*), have all found increased rates of TB disease
52 progression in the setting of low CD4+ T counts, pointing to a critical role for CD4+ T cells in controlling
53 *Mtb* infection. However, efforts to generate vaccines that primarily leverage T cell immunity to drive
54 protection against TB have been met with limited success.

55 The first large-scale TB vaccine clinical trial since BCG was the T_H1-directed MVA-85A vaccine
56 phase 2b trial (*10*). Despite the lack of efficacy of MVA-85A vaccination, a post-hoc correlates analysis
57 of the study found Ag85A-specific IgG responses to be linked with reduced risk of TB disease (*11*),
58 identifying humoral immunity as an unexpected negative correlate of TB disease risk. More recently, the
59 M72/AS01$_E$ phase 2b TB vaccine trial in adults reported a 50% reduction in rates of progression to active
60 TB (ATB) (*12*). While robust T cell immunity was observed following M72-vaccination, strong anti-M72-
61 specific humoral immunity was also observed, as all vaccinees in the M72/AS01$_E$ group remained
62 seropositive 36 months following vaccination (*12*, *13*). Together, these human vaccination studies point

63 to the potential importance of both cellular and humoral immunity in vaccine-mediated protection against
64 TB.

65 In addition to the promising efficacy signals that have begun to emerge in human TB vaccine
66 studies (*13*, *14*), intravenous (IV) BCG vaccination of non-human primates (NHPs) has been shown to
67 provide robust protection against *Mtb* infection (*15–20*). Remarkably, IV BCG vaccination resulted in a
68 100,000-fold reduction in lung bacterial burden compared with standard intradermal BCG vaccination,
69 with six out of ten macaques demonstrating no detectable level of *Mtb* infection (*20*). In contrast, high-
70 dose intradermal BCG and aerosol BCG vaccination regimens resulted in lung bacterial burden levels
71 similar to those observed with standard intradermal BCG vaccination (*20*). IV BCG vaccinated rhesus
72 macaques exhibited increased antigen-responsive CD4 and CD8 T cells systemically, and locally in the
73 lung compared to the other vaccination groups (*20*). Concomitant with enhanced T cell responses, IV BCG
74 vaccinated animals elicited stronger whole-cell lysate reactive antibody responses in the plasma and
75 bronchoalveolar lavage (BAL) fluid (*20*). Yet, while broad differences in antibody responses across BCG
76 vaccination groups were observed in this study, their antigenic targets, functional and anti-microbial
77 activity, and relationship with *Mtb* burden were not defined.

78 Here we leveraged Systems Serology to investigate the antigen-specific humoral immune
79 responses that uniquely evolve following IV BCG vaccination in rhesus macaques (*21*). We demonstrate
80 that compared to standard intradermal BCG vaccination, high dose intradermal BCG vaccination and
81 aerosol BCG vaccination, IV BCG vaccination elicits superior antigen-specific humoral immunity in the
82 periphery, and was the only regimen to induce a robust, lung-compartmentalized antibody response
83 capable of restricting *Mtb* growth *in vitro*. While IgG, IgA, and several Fc-receptor binding antibody
84 subpopulations expanded selectively in the lungs of IV immunized animals, antigen-specific IgM titers
85 were strongly associated with reduced bacterial burden in the BAL and plasma of animals immunized
86 with IV BCG. IgM titers were also found to be a marker of protective immunity in rhesus macaques
87 mucosally vaccinated with an attenuated *Mtb* strain (*Mtb-ΔsigH*) – an orthogonal vaccination strategy also

88 shown to protect rhesus macaques from lethal *Mtb* challenge (*22*). Finally, we show that a LAM-specific
89 IgM monoclonal antibody reduced *Mtb* survival *in vitro*, suggesting that vaccine-induced IgM responses
90 are plausible contributors to vaccine-induced protection against *Mtb*.

91 **RESULTS**

92 **IV BCG immunization drives higher and more durable plasma antigen-specific antibody titers**

93 Following IV BCG immunization, there was a marked increase in *Mtb* whole-cell lysate reactive IgG and
94 IgA titers compared to BCG administration by other routes (*20*). However, in this first study, the antibody
95 responses elicited by the different BCG vaccination strategies to distinct *Mtb* antigen targets were not
96 assessed. Thus, we sought to determine whether particular antigen-specific antibody populations are
97 differentially induced by different BCG vaccination strategies. Antibody levels to a panel of *Mtb* antigens
98 were compared using a custom, multiplexed Luminex assay (*23*). The antigen panel included: purified
99 protein derivative (PPD) – a heterogenous collection of *Mtb* proteins (*24*), lipoarabinomannan (LAM) – a
100 critical cell wall glycolipid (*25*), HspX – a stress induced intracellular protein (*26*), as well as PstS1 and
101 Apa – both cell membrane associated glycoproteins linked to host cell invasion (*27*, *28*). Of note, each of
102 these antigens are expressed by both BCG and *Mtb*. Plasma samples collected pre-vaccination, week 8
103 post-vaccination, time of *Mtb* challenge (week 24), and post-infection (week 28) were analyzed, and fold
104 change in antibody titer over pre-vaccination levels was calculated for each macaque at each timepoint.

105 Following immunization and prior to infection, antigen-specific IgG1 responses were detected in
106 macaques across all vaccine arms. There were weak responses to all antigens in animals receiving standard
107 ID BCG (Fig 1A). Conversely, those that received IV BCG vaccination displayed the largest increase in
108 plasma IgG1 titers to nearly all tested antigens following vaccination. More specifically, PPD, LAM,
109 PstS1, and Apa IgG1 titers in the IV BCG group were each significantly higher than those in the standard
110 ID BCG group both at week 8 post-vaccination, and at the time of *Mtb* challenge (week 24 post-
111 vaccination) (Fig 1A). The additional vaccination groups – high dose intradermal (ID_{high}), aerosol (AE),
112 and aerosol/intradermal (AE/ID) – trended towards higher IgG1 levels compared to the standard ID BCG
113 group, though the differences were only significant for the ID_{high} Apa-specific response (Fig 1A).

114 Antigen-specific IgA responses were also observed following vaccination across each of the
115 experimental BCG vaccination groups, though the fold increases in IgA titer were not as prominent as

116 those for IgG1. IV BCG vaccinated macaques elicited significantly higher IgA titers to LAM and PstS1
117 at week 8 post-vaccination and at the time of *Mtb* challenge compared to the standard ID BCG group,
118 which did not generate a detectable increase in antigen-specific IgA titers to any of the antigens following
119 vaccination (Fig 1B). Animals in the ID_{high} group also elicited a significant increase in LAM IgA titers at
120 week 8 post-vaccination (Fig 1B). However, minimal vaccine-induced plasma IgA responses to the
121 additional antigens were detected in the other groups (Fig 1B).

122 Finally, antigen-specific IgM responses were detected in multiple experimental BCG vaccination
123 groups, with IV and ID_{high} vaccinated macaques mounting the strongest peripheral IgM responses to BCG
124 vaccination. IV BCG vaccinated animals exhibited significantly higher LAM-, PstS1-, and Apa-specific
125 IgM titers at week 8 following vaccination compared to the standard ID BCG group, while responses in
126 the ID_{high} group were not significantly different (Fig 1C). LAM IgM titers also trended higher at the time
127 of challenge in the IV group, though the difference was no longer significant at this timepoint (Fig 1C).

128 Together, these data highlight peripheral differences in the antibody response to specific antigens
129 induced by distinct BCG vaccination strategies. IV BCG immunized animals generated particularly high
130 antigen-specific antibody levels in the plasma, with protein- and LAM-specific antibody responses
131 persisting exclusively in IV immunized animals 24 weeks following vaccination, to the time of *Mtb*
132 challenge. Further, standard ID BCG vaccination generated a weaker antigen-specific antibody response
133 than the experimental vaccination regimens tested – each of which delivered a larger dose of BCG in
134 addition to changing route – suggesting that altering both route and dose may result in enhanced peripheral
135 humoral immune responses to BCG vaccination.

136

137 **IV BCG vaccination uniquely elicits a robust lung-compartmentalized antibody response**

138 We next aimed to profile the antigen-specific humoral immune response at the site of infection using
139 bronchoalveolar lavage fluid (BAL) collected from each macaque pre-vaccination, week 4 post-
140 vaccination, and week 16 post-vaccination – the final timepoint the BAL procedure was performed prior

141 to *Mtb* challenge. IV BCG vaccination uniquely elicited a robust antibody response in the airways
142 following vaccination (Fig 2A – C). Specifically, IV BCG vaccinated animals mounted IgG1, IgA, and
143 IgM responses in the BAL that were significantly higher than the standard ID BCG group at week 4 across
144 all mycobacterial antigens tested (Fig 2A – C). The magnitude of the responses was particularly striking,
145 with over 100-fold increases in antibody levels observed for some IV BCG vaccinated macaques (Fig 2A).
146 Most antibody responses elicited were transient, with only statistically significant levels of LAM-, PstS1-
147 , and Apa-specific antibodies detected in the BAL 16 weeks following vaccination. A small number of
148 macaques in the ID_{high}, AE, and AE/ID groups additionally generated detectable antibody titers in the
149 BAL following BCG vaccination (Fig 2A – C). However, these responses were limited to one or two
150 macaques in each group, and were substantially lower in magnitude than responses generated in IV BCG
151 immunized animals (Fig 2A – C). These data indicate that IV BCG vaccination alone induced strong,
152 lung-compartmentalized, antigen-specific humoral immune responses. These antibodies contracted, but
153 persisted at detectable levels in IV immunized animals for at least 4 months following immunization.
154

155 **Antibodies from IV BCG vaccinated macaques mediate superior innate immune activation**

156 Beyond their ability to bind and recognize pathogens or pathogen-infected cells, antibodies are able to
157 deploy the anti-microbial activity of the innate immune system via Fc:Fc-receptor engagement to control
158 a wide range of microbes (*29*). Further, Fcγ receptor (FcγR) signaling is necessary for the optimal survival
159 and bacterial containment of *Mtb* in mice (*30*). Thus, we next measured the FcγR binding and functional
160 capacity of plasma- and BAL-derived antibodies elicited in each BCG-vaccinated macaque to determine
161 whether certain antibody FcγR binding profiles and/or antibody effector functions selectively tracked with
162 distinct BCG vaccination strategies.

163 In the plasma, the IV BCG group displayed a trend towards higher levels of FcγR binding
164 antibodies than the standard ID BCG group across nearly all antigens measured, including significantly
165 increased PPD-, PstS1-, and Apa-specific FcγR2A and FcγR3A binding antibodies 8 weeks post-

166 vaccination (Fig 3A). Further, although FcγR binding antibodies waned by the time of *Mtb* challenge
167 across all vaccination groups, IV BCG vaccinated macaques maintained significantly higher levels of
168 PPD- and PstS1-specific FcγR2A and FcγR3A binding antibodies close to the time of challenge,
169 suggesting durable antibody functionality in this group (Fig 3A). To examine plasma antigen-specific
170 antibody functionality, antibody-dependent phagocytosis by monocytes and neutrophils, as well as NK
171 cell degranulation assays were performed. Each of these measurements were captured for LAM-specific
172 antibodies, as each BCG vaccination regimen elicited detectable LAM-specific antibody titers in the
173 plasma (Fig 1A – C). Antibodies from IV BCG vaccinated macaques induced the most potent antibody-
174 dependent neutrophil phagocytosis, which was moderately, yet significantly higher than that observed in
175 the standard ID BCG group at week 8 post-vaccination (Fig 3B). In contrast, limited differences were
176 observed in LAM-specific antibody-dependent monocyte phagocytosis and antibody-dependent NK cell
177 degranulation – a surrogate for antibody-dependent cellular cytotoxicity (ADCC) (*31*) – across the vaccine
178 groups (Fig 3B).

179 In line with the elevated antibody levels observed in the BAL of IV BCG vaccinated macaques
180 (Fig 2A – C), antibodies in the IV group demonstrated the highest levels of FcγR binding (Fig 3C). IV
181 BCG immunized animals generated significantly higher levels of LAM-specific FcγR2A binding
182 antibodies at week 4 post-vaccination (Fig 3C). In addition, antigen-specific FcγR3A binding levels in the
183 BAL were particularly robust in the IV vaccinated group, with IV macaques displaying significantly
184 higher levels of FcγR3A binding antibodies to PPD, LAM, PstS1, and Apa 4 weeks following vaccination
185 (Fig 3C). LAM-, and PstS1-specific FcγR3A binding antibody levels remained significantly higher at
186 week 16 post-vaccination (Fig 3C). Furthermore, BAL-derived antibodies in the IV group demonstrated
187 superior LAM-specific functional activity. Specifically, BAL-derived antibodies from IV BCG vaccinated
188 animals exhibited a trend towards stronger antibody-dependent monocyte phagocytosis activity (Fig 3D).
189 More strikingly, the IV BCG group demonstrated significantly higher antibody-dependent neutrophil
190 phagocytosis and NK cell degranulation activity week 4 vaccination, with little functionality observed in

191 the other vaccination groups (Fig 3D). This activity returned to baseline in a majority of animals by week
192 16 post-vaccination (Fig 3D).

193 Previous data have linked an enrichment of FcγR3A binding and NK cell activating antibodies in
194 the setting of LTBI, to enhanced intracellular *Mtb* killing in macrophages (*32*). Therefore, given the
195 expansion of both of these humoral features particularly in the BAL of the IV immunized group 4 weeks
196 post-vaccination, we next examined the anti-microbial activity of antibodies from each vaccination group
197 in this context. Human monocyte-derived macrophages were infected with a live/dead reporter strain of
198 *Mtb* (*33*), followed by the addition of pooled plasma or BAL from each BCG vaccination group. Plasma
199 from the IV group did not drive significant *Mtb* restriction across either of the timepoints (Fig 3E).
200 Conversely, the week 4 IV BCG BAL pool did drive moderate, yet significant intracellular *Mtb* restriction,
201 whereas the ID_{high} BCG BAL pool tended to enhance infection. These patterns were consistently observed
202 across all tested macrophage donors (Fig 3F).

203 Taken together, these data highlight the induction of highly functional antibodies following IV
204 BCG immunization in rhesus macaques. Further, the increases selectively observed in FcγR3A binding,
205 NK cell degranulation, and intracellular *Mtb* killing in the BAL were particularly salient given recent
206 associations reported between both FcγR3A binding, as well as NK cell activity, and improved *Mtb* control
207 (*32*, *34*).

208

209 **Antigen-specific IgM titers in the plasma and BAL negatively correlate with *Mtb* burden**

210 A spectrum of bacterial burden was observed in the lungs of rhesus macaques across the BCG vaccinated
211 groups at the time of necropsy (*20*). Thus, despite IV immunization clearly affording optimal bacterial
212 control following *Mtb* challenge, we next aimed to define whether any antibody features exhibited a robust
213 relationship with lung *Mtb* burden.

214 In the plasma, 5 antibody measurements were significantly negatively associated with *Mtb* burden
215 after multiple hypothesis testing correction (Fig 4A) (*35*). Surprisingly, each of the features identified

216 were antigen-specific IgM titers at week 8 post-vaccination or at the time of challenge (Fig 4A and B),
217 revealing an unexpected significant relationship between plasma antigen-specific IgM titers and improved
218 outcome following *Mtb* challenge. In contrast, while higher antibody titers have historically been
219 associated with elevated antigenic burden and enhanced *Mtb* disease, antibody levels and features were
220 not identified that tracked positively with *Mtb* burden at either significance level (Fig 4A).

221 In the BAL, 18 antibody features were significantly negatively associated with *Mtb* burden after
222 multiple hypothesis testing correction (Fig 4C) (*35*). Several antigen-specific IgG1, IgA, IgM, and FcγR
223 binding measurements in the BAL at 4 or 16 weeks post-vaccination were negatively correlated with *Mtb*
224 levels at the time of necropsy (Fig 4C and D). The majority of these features associated with reduced *Mtb*
225 bacterial burden included antibody features present week 4 post-vaccination, the exception being LAM
226 and PstS1 IgM titers at week 16 (Fig 4C and D). Again, none of the BAL antibody features measured had
227 a significant positive correlation with *Mtb* burden at necropsy at either significance level (Fig 4C).

228 Collectively, the particularly low *Mtb* burden present in IV immunized animals indicate that the
229 relationship observed between select humoral features and bacterial burden track with vaccination route,
230 and thus may not represent independent correlates of protection. Nevertheless, these analyses point to the
231 vaccine-induced humoral immune features which track most closely with improved microbial control in
232 this vaccination cohort. Notably, IgM responses alone tracked with reduced *Mtb* burden close to the time
233 of challenge across both compartments, potentially representing direct mechanistic correlates of
234 immunity, or markers of a unique functional humoral immune response in these animals.

235

236 **Antibody profiles accurately distinguish protected and susceptible BCG-vaccinated macaques**

237 Given that many antibody titer and functional measurements were highly correlated, even across
238 compartments, we next sought to determine whether a minimal set of antibody features could be defined
239 that collectively tracked with *Mtb* control. Thus, macaques with a lung *Mtb* burden at necropsy below
240 1000 were categorized as protected (total n = 11; 9 IV BCG, 1 ID_{high}, 1 AE/ID BCG), and those with an

241 *Mtb* burden greater than or equal to 1000 were categorized as susceptible (total n = 37). Next, least absolute
242 shrinkage and selection operator (LASSO) regularization was implemented on the standardized antibody
243 data, removing variables unrelated to the outcome, as well as reducing the number of highly correlated
244 features (*36*). Partial least squares discriminant analysis (PLS-DA) was then performed to visualize and
245 quantify group separation (*37*, *38*).

246 Robust separation was observed between protected and susceptible macaques on the basis of
247 humoral profile (Fig 4E). The model distinguished protected from susceptible animals with a balanced
248 cross-validation accuracy of 89.6% (Fig 4E). Remarkably, only 3 features were required to achieve this
249 high level of predictive accuracy: BAL HspX-specific IgM at week 4, plasma LAM-specific IgG1 at week
250 8, and plasma LAM-specific IgM at the time of challenge. Each of these features contributed to separation
251 along latent variable 1 (LV1) (Fig 4F). The selection of these three variables across distinct timepoints
252 suggests that substantive humoral differences were present between protected and susceptible BCG-
253 vaccinated macaques beginning in the lung in week 4, extending out to the time of challenge in the plasma.
254 Further, this analysis demonstrates that protected and susceptible BCG-vaccinated macaques can be
255 accurately resolved by simply using antibody titer measurements.

256

257 **Protective vaccination via attenuated *Mtb* is associated with increased plasma IgM titers**

258 While our analyses identified humoral features associated with reduced *Mtb* burden in BCG immunized
259 animals, because vaccination route was so closely linked to protection in this cohort, the generalizability
260 of these findings was unclear. Thus, we next queried whether similar humoral features were associated
261 with *Mtb* control in an independent *Mtb* vaccination study in NHPs. Previous work demonstrated that AE
262 vaccination with an attenuated *Mtb* strain (*Mtb-ΔsigH*) provided superior protection compared to AE BCG
263 vaccination in rhesus macaques (*22*). Thus, antibody profiling was performed on the plasma of *Mtb-ΔsigH*
264 or AE BCG vaccinated animals.

265 Using antibody titer measurements alone, *Mtb-ΔsigH* and BCG vaccination groups could be
266 clearly separated using a principal component analysis (PCA) (Fig 5A). Analysis of the PCA loadings plot
267 revealed that antigen-specific IgM responses primarily drove separation between the two groups, with
268 antigen-specific IgM responses enriched among protected *Mtb-ΔsigH* vaccinated macaques (Fig 5B).
269 Similarly, univariate analyses indicated that *Mtb-ΔsigH* vaccinated macaques elicited significantly higher
270 LAM-specific IgM titers week 7 post-vaccination, as well as a trend towards increased Apa- and HspX-
271 specific IgM titers (Fig 5C). In contrast, minimal differences in antigen-specific IgG1 and IgA titers were
272 noted between the *Mtb-ΔsigH* and BCG groups (Fig S4). Finally, antibody responses to the Ebola virus
273 negative control antigen were not detected in either group as expected regardless of isotype (Figs 5C and
274 S4).

275 Thus, although the sample size from this cohort is small, increased plasma antigen-specific IgM
276 titers tracked with reduced *Mtb* disease. A result similar to that observed in BCG immunized animals (Fig
277 4A), potentially hinting at a common association between antigen-specific IgM and vaccine-induced *Mtb*
278 control.

279

280 **Superior *in vitro* anti-microbial effect of LAM-specific IgM**

281 Data from both the BCG route and the *Mtb-ΔsigH* immunization study pointed to an unexpected
282 association of antigen-specific IgM titers with improved vaccine-induced *Mtb* control. However, whether
283 elevated IgM levels represented a biomarker or contributed directly to anti-microbial control remained
284 unclear. Given the emerging data pointing to an anti-microbial role for polyclonal IgG and monoclonal
285 IgG and IgA antibodies against *Mtb* (*32*, *39–44*), we next queried whether IgM also might harbor some
286 anti-microbial capacity, using an engineered high-affinity LAM-specific antibody clone (A194) generated
287 as an IgG1 and as an IgM (*45*).

288 In light of the previous observation that IgG1- and IgM-rich BAL from IV immunized rhesus
289 macaques could drive intracellular *Mtb* killing in macrophages (Fig 3F), we first compared the anti-

290 microbial activity of each isotype in a similar human monocyte-derived macrophage model. However,
291 despite the anti-microbial signal observed in the BAL of IV BCG immunized animals, neither LAM-
292 specific monoclonal antibody drove significant intracellular *Mtb* restriction in macrophages when added
293 post-infection (Fig 6A).

294 While macrophages represent a primary cellular niche for *Mtb in vivo* during infection, we also
295 probed the anti-microbial role for each LAM-specific antibody in a whole-blood model of infection – a
296 system which queries the broader role of multiple immune cell types and components in microbial
297 restriction. Specifically, fresh blood from healthy human donors was simultaneously infected with an *Mtb*
298 luciferase reporter strain (*46*), and treated with each LAM-specific monoclonal antibody. Luminescence
299 readings were then taken to obtain *Mtb* growth curves in the presence of each antibody treatment over the
300 course of 120 hours. Remarkably, only the LAM-specific IgM antibody drove significant *Mtb* restriction
301 in this system (Fig 6B). Further, the LAM-specific IgM antibody drove improved bacterial restriction
302 compared to the IgG1 across nearly every donor tested (Fig 6B).

303 Ultimately, these data demonstrate that a high-affinity LAM-specific antibody clone drives
304 improved *Mtb* restriction in whole-blood as an IgM, as compared an IgG1 variant, suggesting that in
305 addition to representing an early marker of vaccine-induced *Mtb* control, *Mtb*-specific IgM antibodies
306 have the potential to functionally contribute to immunologic control of *Mtb*.

307 **DISCUSSION**

308 Recently, IV BCG vaccination in rhesus macaques was shown to result in robust protection against
309 *Mtb* challenge (*20*), providing a unique opportunity to interrogate immunologic correlates and
310 mechanisms of protection against *Mtb*. While published data highlighted the robust T cell immunity
311 observed following IV BCG immunization, strong *Mtb* whole-cell lysate reactive humoral immune
312 responses were also noted following this distinct vaccine delivery strategy (*20*). Given our emerging
313 appreciation for a potential role for humoral immunity in *Mtb* control (*47*), here we deeply probed the
314 antigen-specific humoral immune response across multiple BCG vaccine routes and doses to determine
315 whether specific humoral immune profiles may complement cellular immunity, and potentially contribute
316 to the protection afforded by IV BCG. Elevated antigen-specific antibody titers were observed in both the
317 plasma and the lungs of IV BCG vaccinated animals, with a significant expansion of functional and anti-
318 microbial responses in the BAL. Unexpectedly, correlation analyses revealed the unique association of
319 BAL and plasma IgM responses close to or at the time of challenge, with reduced *Mtb* burden at necropsy
320 in BCG immunized animals. Moreover, expanded plasma IgM titers were also observed in macaques
321 immunized with an orthogonal, attenuated *Mtb* strain (*Mtb-ΔsigH*) that also conferred enhanced control
322 over *Mtb* (*22*). Finally, a LAM-specific IgM antibody resulted in enhanced restrictive activity of *Mtb in*
323 *vitro* compared to the same antibody clone with an IgG1 heavy chain, collectively pointing to a potential
324 role for *Mtb*-specific IgM as a novel mechanistic correlate of protection in vaccine-induced *Mtb* control.

325 IV BCG immunized animals generated the strongest and most durable peripheral antibody
326 responses directed to both protein antigens and to LAM. Conversely, standard ID BCG vaccination
327 generated weaker antibody responses than the experimental vaccination regimens tested – each of which
328 administered a larger dose of BCG (Fig 1). This pattern suggests that increased peak antibody titers may
329 be a consequence of larger BCG dose delivered to these animals during immunization. However, each
330 type of vaccination included in this study – intradermal, aerosol, and IV – additionally resulted in a distinct
331 anatomic localization of vaccine antigen, where IV immunization resulted in robust localization in the

332 spleen (*20*), a primary site of B cell activation (*48*). Thus, it is conceivable that an enrichment of antigen
333 particularly in this primary B cell inductive site, may contribute to the strong and long-lasting peripheral
334 humoral immunity uniquely observed in IV BCG immunized animals.

335 Peripheral antibody titers, often of the IgG isotype, represent a primary correlate of protection for
336 the majority of approved vaccines (*47*, *49–55*). Yet surprisingly, vaccine-specific IgM titers were the only
337 plasma antibody features to correlate inversely with *Mtb* burden in BCG immunized animals (Fig 4).
338 Because protection was so dominantly associated with vaccination regimen, IgM titers did not represent
339 an independent correlate of protection in the BCG route study. However, the potential value of IgM as a
340 mechanistic correlate of immunity was corroborated by an enrichment in plasma IgM responses in animals
341 that demonstrated enhanced *Mtb* control following *Mtb-ΔsigH* immunization (*22*). IgM plays a critical
342 role during infection – particularly in the defense against other encapsulated bacteria – efficiently capable
343 of driving phagocytosis, agglutination, and complement activation (*56*, *57*). IgM has also been recently
344 implicated as a critical regulator of T cell immune responses (*58*), raising the prospect of both direct anti-
345 microbial, and indirect cellular regulatory roles for IgM in immunity against *Mtb.*

346 In the present study, we observed that a high-affinity LAM-specific antibody exhibited superior
347 anti-microbial activity in primary human whole-blood as an IgM compared to as an IgG1. Unlike IgM
348 antibodies that are elicited by vaccination or infection, this IgM monoclonal was an engineered form of a
349 relatively high affinity IgG antibody (A194-01) (*45*, *59–61*). While it is unclear whether IgM antibodies
350 following IV BCG or *Mtb-ΔsigH* immunization require a similarly high affinity to drive anti-microbial
351 function, the *in vitro* anti-microbial impact of this monoclonal suggests that IgM may not only serve as a
352 surrogate of protective vaccine-induced immunity against *Mtb*, but may also play an unexpected
353 mechanistic role in combating *Mtb* infection. Interestingly, several IgM LAM-specific monoclonal
354 antibodies have been isolated from TB patients that also bind with moderate affinities, but not when
355 expressed with an IgG heavy chain (*45*), suggesting that the increase in avidity provided by multimeric
356 IgM may allow the antibody to access epitopes or drive Fc-mediated functions key to protective humoral

357 immunity. Notwithstanding, future work should continue to dissect the mechanistic basis for this *Mtb*
358 restriction activity – including Fab- and Fc-mediated mechanisms through which IgM may contribute to
359 protection.

360 Beyond superior plasma antibody responses, IV BCG immunization was uniquely associated with
361 a significant increase in BAL IgG1, IgA, and IgM antibody titers to all mycobacterial antigens tested at
362 week 4 post-vaccination. Despite the highly functional nature of the BAL-derived antibodies following
363 IV BCG vaccination, it remains unclear whether enhanced antibody titers and functions present in the
364 BAL represent a signature of protection, a signature of IV vaccination, or both. Follow-up studies, using
365 reduced dosing of IV BCG, may provide critical clues required to uncover the quantitative and qualitative
366 correlates of immunity against *Mtb*. However, rhesus macaques vaccinated with repeated low-dose
367 endobronchial instillation of BCG exhibited increased protection against *Mtb* challenge compared to
368 macaques vaccinated with standard ID BCG (*62*). These protected animals exhibited significantly higher
369 PPD-specific antibody titers in the BAL compared to animals that received intradermal BCG
370 immunization. While only PPD-specific IgA and PPD-specific pan-isotype antibodies were measured,
371 these results point again to robust lung-residing humoral immune responses as a common immune
372 signature of protection between these two studies and across vaccination strategies. Notably, both
373 intravenous and endobronchially instilled BCG have been shown to drive substantial BCG deposition in
374 the lungs (*20*). As such, it is possible that the localization of vaccine antigen deep in lungs – rather than
375 in the dermis by ID vaccination, or in the upper respiratory tract by AE vaccination – may be critical for
376 the induction of robust, lung-specific T and B cell immunity, that may work together to interrupt infection.

377 Lastly, despite the potent lung antibody responses observed in IV BCG immunized animals, the
378 BAL antibody titers, functionality, and anti-microbial activity were largely transient (Figs 2 and 3). Thus,
379 unlike lung T cell responses, which remained expanded over the course of the entire vaccination study
380 (*20*), antibodies were less abundant in the lungs at the time of *Mtb* challenge (week 24). Critically, while
381 differences may exist between BAL-derived antibodies and those found in the lung parenchyma, select

382 antibody features – including LAM-specific IgG1, IgA, IgM titers, and LAM-specific FcγR3A binding
383 antibodies – remained detectable and significantly higher in the airways of the IV group close to challenge.
384 Given the small number of bacteria used in challenge (10 CFUs) (*20*), as well as the limited number of
385 bacteria believed to cause infection in humans (*63*), it is plausible that even low levels of antibodies at the
386 site of infection may be sufficient to capture the pathogen and contribute to first line defense. Of note,
387 work in the context of influenza has demonstrated that vaccine-induced lung-resident memory B cell cells
388 – particularly IgM+ memory B cells – may also play a critical role in rapid response to infection, swiftly
389 generating antibody-secreting cells that rapidly re-populate the lung with antibodies able to control and
390 clear infection (*64*, *65*). Thus, it is conceivable that antibodies present in the airways 4 weeks post-
391 vaccination, mark the establishment of lung-resident B cell immunity, which could respond
392 instantaneously to *Mtb* challenge and contribute to protection in coordination with lung-resident T cell
393 responses.

394 Ultimately, taken together, this work illustrates that IV BCG immunization drives superior plasma
395 and lung antibody responses compared to ID and AE BCG vaccination. Specific humoral features
396 associated with protection were identified across studies, highlighting potentially conserved roles for
397 antibodies in vaccine-mediated protection against *Mtb*. Because of the potential safety issues associated
398 with IV immunization, the development of alternative vaccination strategies able to mimic the protective
399 humoral immune responses identified herein, may obviate the need for IV immunization to drive
400 protection against TB in human populations. Thus, while efforts to leverage the immune response to
401 combat TB via vaccination have largely focused on cellular immunity, this work demonstrates the value
402 of a comprehensive examination of antibody characteristics across TB vaccine platforms, and motivates
403 the continued study of antibodies as markers, and as functional mediators of protection against TB.

404 **MATERIALS AND METHODS**

405 **Study design**

406 Rhesus macaque (*Macaca mulatta*) plasma and bronchoalveolar lavage fluid (BAL) samples from the
407 BCG route vaccination cohort were collected during a study performed at the Vaccine Research Center at
408 the National Institutes of Health (*20*). All experimentation and sample collection from the original study
409 complied with ethical regulations at the respective institutions (*20*). 48 BCG immunized animals were
410 included in the study including: 10 animals that received standard intradermal (ID) BCG vaccination
411 (target dose: 5×10^5 CFUs), 8 animals that received high-dose intradermal (ID_{high}) BCG vaccination
412 (target dose: 5×10^7 CFUs), 10 animals that received intravenous (IV) BCG vaccination (target dose: $5 \times$
413 10^7 CFUs), 10 animals that received aerosol (AE) BCG vaccination (target dose: 5×10^7 CFUs), and 10
414 animals that received a combination of AE and standard ID (AE/ID) BCG vaccination (target dose: AE 5
415 $\times 10^7$ CFUs, ID 5×10^5 CFUs) (*20*). Following BCG vaccination, each macaque was challenged with 10
416 CFUs of *Mtb Erdman*, with a study endpoint of 12 weeks following *Mtb* challenge (*20*). In this study, *Mtb*
417 burden values used throughout represent total thoracic CFUs measured at necropsy in the original study,
418 and were measured as described previously (*20*). Plasma samples were analyzed from the following
419 timepoints: pre-vaccination, week 8 post BCG vaccination, time of challenge (week 24 post BCG
420 vaccination), and week 28 (4 weeks post *Mtb* challenge). BAL samples were analyzed from the following
421 timepoints: pre-vaccination, week 4 post BCG vaccination, and week 16 post BCG vaccination. BAL was
422 received as a 10X concentrate, and further diluted for experiments.

423 Rhesus macaque plasma samples from the attenuated *Mtb* vaccination cohort were collected during
424 a study performed at the Tulane National Primate Research Center (*22*). All experimentation and sample
425 collection from the original study were approved by the Institutional Animal Care and Use Committee
426 and were performed in strict accordance with National Institutes of Health guidelines (*22*). Plasma from
427 9 rhesus macaques were analyzed in the present study. 4 animals received AE BCG vaccination (target
428 dose: 1,000 CFUs), and 5 animals received AE *Mtb-ΔsigH* – an attenuated *Mtb* strain in the CDC1551

429 genetic background – vaccination (target dose: 1,000 CFUs). Eight weeks post-vaccination, each animal
430 was challenged with a target dose of 1,000 CFUs of *Mtb CDC1551* (*22*). Plasma samples were analyzed
431 from the following timepoints: pre-vaccination, week 7 post-vaccination, and necropsy (week 15).
432
433 **Antigens**
434 To profile humoral immune responses, a panel of BCG/*Mtb*-antigens were used: purified protein
435 derivative (PPD) (Statens Serum Institute), HspX (provided by T. Ottenhoff), LAM (BEI Resources, NR-
436 14848), PstS1 (BEI Resources, NR-14859), and Apa (BEI Resources, NR-14862). Zaire ebolavirus
437 glycoprotein (R&D Systems) was used as a negative control for the attenuated *Mtb* analysis.
438
439 **Non-human primate reagents**
440 Mouse anti-rhesus IgG1 (clone 7H11) and IgA (clone 9B9) secondary antibodies were obtained from the
441 National Institutes of Health Nonhuman Primate Reagent Resource supported by AI126683 and
442 OD010976. Mouse anti-monkey IgM (clone 2C11-1-5) was acquired from Life Diagnostics. Soluble
443 rhesus macaque FcγR2A and FcγR3A were acquired from the Duke Human Vaccine Institute Protein
444 Production Facility.
445
446 **Antigen-specific antibody levels**
447 Magnetic carboxylated fluorescent beads of distinct regions (Luminex Corp.) were first coupled to each
448 protein antigen in a two-step carbodiimide reaction as described previously (*23*). LAM was modified by
449 4-(4,6-dimethoxy[1,3,5]triazin-2-yl)-4-methyl-morpholinium (DMTMM) and coupled to Luminex
450 magnetic carboxylated fluorescent beads using protocols described previously (*66*, *67*).
451 Luminex using antigen-coupled beads to measure relative levels of antigen-specific antibodies was
452 then performed as described previously (*68*), with minor modifications. A master mix of antigen-coupled
453 beads was made at a concentration of 16.67 beads per µL per region in 0.1% bovine serum albumin (BSA)-

454 PBS, and 750 beads per region per well (45uL) were added to a clear, flat-bottom 384 well plate (Greiner).
455 5µL of diluted sample was then added to the wells. Plasma from the BCG route vaccination study was
456 diluted and run at 1:10 and 1:100. The 1:100 dilution was utilized for LAM IgG1, Apa IgG1, LAM IgA,
457 and all IgM antigens. The 1:10 dilution was utilized for the remaining conditions. BAL from the BCG
458 route vaccination study was diluted as follows: IgG1 1X, IgA 1X, IgM 0.1X. Plasma from the attenuated
459 *Mtb* vaccination study was diluted as follows: IgG1 1:150, IgA 1:150, IgM 1:750. After adding the diluted
460 samples, the plate was incubated shaking at 700 RPM overnight at 4°C. Next, the plate was washed 6
461 times and 45uL of mouse anti-rhesus IgG1, IgA, or IgM antibody at 0.65ug/mL was added, and incubated
462 shaking at 700 RPM at room temperature (RT) for 1 hour. The plate was then washed 6 times and 45uL
463 of Phycoerythrin (PE)-conjugated goat anti-mouse IgG was added (ThermoFisher, 31861) and incubated
464 shaking at 700RPM at RT for 1 hour. The plate was then washed 6 times, and resuspended in Sheath Fluid
465 (Luminex Corp.) in a final volume of 60uL. PE median fluorescence intensity (MFI) levels were then
466 measured via the FlexMap 3D (Luminex Corp.) Data are represented as fold change over pre-vaccination
467 levels. Samples were measured in duplicate.
468
469 **Antigen-specific Fcγ receptor binding**
470 Rhesus macaque FcγRs were biotinylated as described previously (*68*). In brief, each FcγR was
471 biotinylated using a BirA biotin-protein ligase bulk reaction kit (Avidity) according to the protocol of the
472 manufacturer, and excess biotin was removed using 3 kD cutoff centrifugal filter units (Amicon).
473 Luminex using biotinylated rhesus macaque FcγRs and antigen-coupled beads to measure relative
474 binding levels of antigen-specific antibodies to FcγRs was then performed as described previously (*68*),
475 with minor modifications. A master mix of antigen-coupled beads was made at a concentration of 16.67
476 beads per µL per region in 0.1% BSA-PBS, and 750 beads per region per well (45uL) were added to a
477 clear, flat-bottom 384 well plate (Greiner). 5µL of sample (Plasma: FcγR2A 1:10, FcγR3A 1:10; BAL:
478 FcγR2A 1X, FcγR3A 1X) was added to the wells and incubated shaking at 700 RPM overnight at 4°C.

479 After overnight incubation, streptavidin-PE (ProZyme) was added to each biotinylated FcγR in a 4:1 molar
480 ratio and incubated rotating for 10 minutes at RT. 500µM biotin was then added at 1:100 relative to the
481 total solution volume to quench the extra streptavidin-PE, and incubated rotating for 10 minutes at RT.
482 After washing the assay plate 6 times, 40µL of each prepared detection FcγR (1µg/ml in 0.1% BSA-PBS)
483 was added to the immune-complexed microspheres and incubated shaking at 700 RPM for 1 hour at RT.
484 The plate was then washed 6 times, and resuspended in Sheath Fluid (Luminex Corp.) in a final volume
485 of 60uL. PE MFI levels were then measured via the FlexMap 3D (Luminex Corp.). Data represented as
486 fold change over pre-vaccination level. Samples were measured in duplicate.
487
488 **Antibody-dependent cellular phagocytosis (ADCP)**
489 PPD ADCP (data not shown) was measured as described previously (*32*, *69*). LAM ADCP was measured
490 as described previously (*32*, *69*) with minor changes. For every 100ug of LAM (dissolved in ddH_2O),
491 10uL of 1M sodium acetate (NaOAc), and 2.2uL of 50mM sodium periodate ($NaIO_4$) was added. This
492 oxidation reaction proceeded for 45 – 60min on ice in the dark. 12uL of 0.8M $NaIO_4$ was then added to
493 block oxidation, and the solution was incubated for 5 min at RT in the dark. Next, the oxidized LAM was
494 transferred to a new tube, and 10uL of 1M NaOAc and 22uL of 50mM hydrazide biotin (Sigma) were
495 added. This biotinylation reaction proceeded for 2 hours at RT. Excess biotin was then removed using
496 Amicon Ultra 0.5.L columns (3K, Millipore Sigma) according to the instructions of the manufacturer.
497 Biotinylated LAM was then added to FITC-conjugated neutravidin beads (Invitrogen, 1.0µm) at a ratio of
498 1µg antigen: 4µL beads, and incubated for overnight at 4°C. Excess antigen was washed away. Antigen-
499 coated beads were incubated with 10uL of sample (plasma 1:10, BAL 1:1) for 2 hr at 37 °C. THP-1 cells
500 (5×10^4 per well) were added and incubated at 37 °C for 16 hr. Bead uptake was measured in fixed cells
501 using flow cytometry on a BD LSRII (BD Biosciences) and analyzed by FlowJo 10.3. Phagocytic scores
502 were calculated as: ((%FITC positive cells) x (geometric mean fluorescence intensity of the FITC positive

503 cells)) divided by 10,000. Data are represented as fold change over pre-vaccination levels. Samples were
504 run in duplicate.
505
506 **Antibody-dependent neutrophil phagocytosis (ADNP)**
507 ADNP was performed as described previously (*70*), with minor changes. LAM was biotinylated and
508 coupled to fluorescent neutravidin beads (1.0µm, Invitrogen), incubated with serum, and washed as
509 described above for ADCP. During the 2-hour bead and serum incubation, fresh peripheral blood collected
510 from healthy donors in acid citrate dextrose (ACD) anti-coagulant tubes was added at a 1:9 ratio to ACK
511 lysis buffer (150mM NH_4Cl, 8610mM $KHCO_3$, 0.1mM Na_2-EDTA, pH 7.4) for 5 minutes at RT. After
512 red blood cell lysis, the blood was centrifuged for 5 minutes at 1500 RPM. After centrifugation,
513 supernatant was removed, and leukocytes were washed with 50ml of 4°C PBS, spun for 5 minutes at 1500
514 rpm and resuspended in R10 medium – (RPMI (Sigma), 10% fetal bovine serum (Sigma), 10mM HEPES
515 (Corning), 2mM L-glutamine (Corning)) – at a final concentration of 2.5 x 10^5 cells/mL. Leukocytes (5 x
516 10^4 cells/well) were then added to the immune-complexed beads and incubated for 1 hour at 37°C 5%
517 CO_2. Following this incubation, the plates were spun for 5 minutes at 500 x g. After removing the
518 supernatant, anti-human CD66b-Pacific Blue (BioLegend) was added to the leukocytes, and the cells were
519 incubated for 20 minutes at RT. Following this incubation, the cells were washed with PBS and fixed.
520 Bead uptake was measured in fixed cells using flow cytometry on a BD LSRII (BD Biosciences) and
521 analyzed by FlowJo 10.3. Phagocytic scores were calculated in the CD66b positive cell population. Data
522 represented as fold change over pre-vaccination level. Samples were run in duplicate.
523
524 **Antibody-dependent NK cell activation (ADNKA)**
525 ADNKA was performed as described previously (*32*), with minor changes. ELISA plates (Thermo Fisher,
526 NUNC MaxiSorp flat bottom) were coated with 150ng/well of LAM and incubated overnight at 4°C. The
527 plates were then washed with PBS and blocked with 5% BSA-PBS for 2 hours. Next, the plates were

528 washed with PBS, and 50uL of sample (plasma 1:10, BAL 1X) was added and incubated for 2 hours at
529 37°C. One day prior to adding the diluted sample, NK cells were isolated from healthy donors using the
530 RosetteSep human NK cell enrichment cocktail (Stemcell) and Sepmate conical tubes (Stemcell)
531 according to the instructions of the manufacturer. Following isolation, NK cells were incubated overnight
532 at 1.5 x 10^6 cells/mL in R10 media with 1ng/mL human recombinant IL-15 (Stemcell). After the 2 hour
533 serum incubation, the assay plates were washed, and 50,000 primary human NK cells, together with 2.5uL
534 PE-Cy5 anti-human CD107a (BD), 0.4uL Brefeldin A (5mg/ml, Sigma), and 10uL GolgiStop (BD) were
535 added to each well of the assay plates. The plates were then incubated for 5 hours at 37°C. Following the
536 incubation, the samples from each well were stained with 1uL each of: PE-Cy7 anti-human CD56, APC-
537 Cy7 anti-human CD16, and Alexa Fluor 700 anti-human CD3 (all from BD). After a 20 minute incubation
538 at RT to allow extracellular staining, the plate was washed with PBS, and the cells were fixed using Perm
539 A and Perm B (Invitrogen). The Perm B solution additionally contained PE anti-human MIP-1β, and APC
540 anti-human IFNγ (both from BD) to allow intracellular cytokine staining. After a final wash in PBS, the
541 cells were resuspended in PBS and the fluorescence of each marker was measured on a BD LSR II flow
542 cytometer (BD Biosciences) and analyzed by FlowJo 10.3. NK cells were defined as CD3 negative, CD16
543 positive, CD56 positive cells. Data are represented as fold change over pre-vaccination levels. The assay
544 was performed in biological duplicate using NK cells from 2 different donors.
545

546 **Macrophage restriction assay (*Mtb-live/dead*)**

547 *In vitro* macrophage *Mtb* survival was measured as described previously (*32*), with minor changes. CD14
548 positive cells were isolated from HIV negative donors using the EasySep CD14 Selection Kit II according
549 to the instructions of the manufacturer (Stemcell). CD14 positive cells were matured for 7 days in R10
550 media without phenol in low adherent flasks (Corning). Monocyte-derived macrophages (MDMs) were
551 plated 50,000 cells per well in glass bottom, 96-well plates (Greiner) 24 hours prior to infection. A reporter
552 *Mtb* strain (*Mtb-live/dead*) with constitutive mCherry expression and inducible green fluorescent protein

553 (GFP) expression (*33*), was cultured in log phase and filtered through a 5µm filter (Milliplex) prior to
554 MDM infection at a multiplicity of infection of 1 for 14 hours at 37°C. Extracellular bacteria were washed
555 off, and 200uL of pooled sample from each of the vaccination groups diluted in R10 without phenol
556 (plasma 1:100, BAL 1X) was added. 3 days following infection, anhydrotetracycline (Sigma) (200 ng/ml)
557 was added for 16 hours to induce GFP expression. 96 hours following infection, cells were fixed and
558 stained with DAPI. Data were analyzed using the Columbus Image Data Storage and Analysis System.
559 Bacterial survival was calculated as the ratio of live to total bacteria (the number of GFP+ pixels (live)
560 divided by the number of mCherry+ pixels (total burden)) within macrophages in each well. Bacterial
561 survival for each condition was normalized by bacterial survival in the no antibody condition. The assay
562 was performed in technical triplicate using MDMs from 4 different donors.
563
564 **Macrophage restriction assay (*Mtb-276*)**
565 CD14 positive cells were isolated from HIV negative donors using the EasySep CD14 Selection Kit II
566 according to the instructions of the manufacturer (Stemcell). CD14 positive cells were matured for 7 days
567 in R10 media without phenol in low adherent flasks (Corning). MDMs were plated 50,000 cells per well
568 in sterile, white, flat-bottom 96-well plate plates (Greiner) 24 hours prior to infection. An auto-luminescent
569 *Mtb* reporter strain (*Mtb-276*) (*46*), was cultured in log phase and filtered through a 5µm filter (Milliplex)
570 prior to MDM infection at a multiplicity of infection of 1, for 14 hours at 37°C. Extracellular bacteria
571 were washed off, and each antibody treatment was diluted to 50ug/mL in R10 without phenol, and 200uL
572 of diluted antibody was added to each MDM-containing well. Control treatments: rifampin (Sigma) at
573 1ug/mL, human IgG1 isotype control (BE0297, BioXcell) at 50ug/mL, and human IgM isotype control
574 (31146, Invitrogen) at 50ug/mL. Luminescence readings were then taken every 24 hours, up to 120 hours
575 following infection to obtain *Mtb* growth curves in the presence of each antibody treatment. Area under
576 the curve values were then computed for each antibody treatment in GraphPad Prism (version 8.4.0).
577

578 **Whole-blood restriction assay**

579 Whole-blood from HIV negative human donors was collected fresh the day of the experiment in acid
580 citrate dextrose tubes. *Mtb-276* previously cultured in 7H9 media at 37ºC in log phase was washed once
581 and resuspended in R10 media without phenol. Whole-blood was then infected with *Mtb-276* such that
582 the final concentration was $1x10^6$ bacteria per mL of blood. Immediately after adding *Mtb-276* to blood,
583 150uL of blood and 150uL of antibody samples pre-diluted to 50ug/mL in R10 media are added together
584 into a sterile, white, flat-bottom 96-well plate in triplicate (Greiner). Final concentration of experimental
585 antibody treatments: 25ug/mL. Final concentration of control treatments: rifampin (Sigma) 0.25ug/mL,
586 human IgG1 isotype control (BE0297, BioXcell) 25ug/mL, and human IgM isotype control (31146,
587 Invitrogen) 25ug/mL. Samples in each well are mixed, then the first luminescence reading is taken on a
588 plate reader (Tecan Spark 10M). The plate is then incubated at 37ºC. Every 24 hours post-infection for
589 120 hours, the samples in each well are mixed, and luminescence readings are taken on a plate reader to
590 obtain *Mtb* growth curves in the presence of different antibody treatments. *Mtb* restriction in whole-blood
591 is calculated as the area under the curve for each condition. Area under the curve values were computed
592 for each antibody treatment in GraphPad Prism (version 8.4.0).

593

594 **LAM-specific monoclonal antibody expression**

595 A194 LAM-specific antibodies were generated as described previously (*45*). In brief, A194-IgG1 was
596 generated by transfecting the A194-IGG1VH and IGVK plasmids into Expi293 cells. A194-IgM was
597 generated by transfecting the A194-IGM1VH, IGVK, and joining (J) chain plasmids into Expi293 cells
598 to generate multimeric IgM. Each antibody was purified by affinity chromatography. Protein A beads and
599 protein L beads were used for the purification of IgG1 and IgM respectively. The antibodies were eluted
600 using a low pH buffer, and characterized by SDS-PAGE for purity and size.

601

602 **Partial least squares discriminant analysis (PLS-DA)**

603 A multivariate model to distinguish protected and susceptible macaques was generated using a
604 combination of least absolute shrinkage and selection operator (LASSO)-based feature selection (*36*, *71*),
605 and partial least squares discriminant analysis (PLS-DA) (*37*, *38*). Protected macaques were defined as
606 those with an *Mtb* burden less than 1000 CFU/mL at time of necropsy. *Mtb* burden values used represent
607 total thoracic CFUs measured at necropsy in the original study, and were measured as described previously
608 (*20*).

609 For feature selection, the data were z-scored and 100 bootstrap datasets were generated. A LASSO
610 model in which the optimal penalty term lambda was chosen via 5-fold cross-validation, was then fit on
611 each bootstrap dataset, and coefficients from each iteration of LASSO regularization were stored. Using
612 these coefficients, variable inclusion probabilities – defined as the proportion of bootstrap replications in
613 which a coefficient estimate is non-zero – were computed for each antibody feature. LASSO
614 regularization was implemented using the glmnet package (version 3.0-2) in R (version 3.6.2).

615 PLS-DA models across a grid of variable inclusion probability cutoffs were fit in a 5-fold cross-
616 validation framework repeated 100 times. Model accuracy – defined as ((1 – balanced error rate) x 100) –
617 was computed for each. The optimal model, which contained 3 antibody features, was found at a variable
618 inclusion probability of 0.45. A graph of the first and second latent variable (LV) from the optimal PLS-
619 DA model is included, as is a variable importance in the projection (VIP) plot, indicating the relative
620 contribution of individual features to separation along the first LV. The significance of the model was
621 assessed using a permutation test. Specifically, the group labels of the macaques were randomly permuted.
622 PLS-DA models were then fit and evaluated for model accuracy in a 5-fold cross-validation framework
623 repeated 100 times. The accuracy of the real model was compared with that of the permuted model using
624 a Mann-Whitney U test. PLS-DA models were implemented using the mixOmics package (version 6.10.9)
625 in R (version 3.6.2).

626

627 **Statistics**

628 For the antibody titer (Fig 1 and 2), FcγR binding (Fig 3 and S1), and functional measurements (Fig 3),
629 from the BCG dose vaccination cohort, Kruskal-Wallis with Dunn's multiple-comparison tests were
630 performed on the fold change values at each timepoint, comparing each vaccination group to the standard
631 ID BCG group. For the macrophage *Mtb* restriction assay (Fig 3), a repeated measures ANOVA with
632 Dunnett's multiple comparisons test was performed for each vaccination group, comparing pre-
633 vaccination restrictive activity with that of each post-vaccination timepoint. For antibody titers in the
634 attenuated *Mtb* vaccination cohort (*Mtb-ΔsigH*) (Fig 5 and S2), Mann-Whitney U tests were performed on
635 the fold change values at each timepoint, comparing aerosol *Mtb-ΔsigH* to the aerosol BCG group. For
636 the LAM-specific monoclonal antibody *Mtb* restriction assays, a repeated measures ANOVA with Sidak's
637 multiple comparisons test was performed to make the relevant statistical comparisons. These statistics
638 were performed in GraphPad Prism (version 8.4.0). Spearman correlations between *Mtb* burden and
639 individual antibody features were computed in R (version 3.6.2) (Fig 4). Adjusted p-values (q-values)
640 were calculated using the Benjamini-Hochberg procedure (*35*).
641
642
643
644
645
646
647
648
649
650
651
652

653 **REFERENCES**

654 1. World Health Organization, "WHO | Global Tuberculosis Report 2020" (2020).

655 2. World Health Organization, "Global Tuberculosis Report" (2019).

656 3. P. E. Fine, Variation in protection by BCG: implications of and for heterologous immunity. *Lancet*
657 *(London, England)*. **346**, 1339–45 (1995).

658 4. A. M. Caruso, N. Serbina, E. Klein, K. Triebold, B. R. Bloom, J. L. Flynn, Mice deficient in CD4
659 T cells have only transiently diminished levels of IFN-gamma, yet succumb to tuberculosis. *J.*
660 *Immunol.* **162**, 5407–16 (1999).

661 5. S. Yao, D. Huang, C. Y. Chen, L. Halliday, R. C. Wang, Z. W. Chen, CD4 $^{+}$ T Cells Contain Early
662 Extrapulmonary Tuberculosis (TB) Dissemination and Rapid TB Progression and Sustain
663 Multieffector Functions of CD8 $^{+}$ T and CD3 $^{-}$ Lymphocytes: Mechanisms of CD4 $^{+}$ T Cell
664 Immunity. *J. Immunol.* **192**, 2120–2132 (2014).

665 6. P. L. Lin, T. Rutledge, A. M. Green, M. Bigbee, C. Fuhrman, E. Klein, J. L. Flynn, CD4 T cell
666 depletion exacerbates acute Mycobacterium tuberculosis while reactivation of latent infection is
667 dependent on severity of tissue depletion in cynomolgus macaques. *AIDS Res. Hum. Retroviruses*.
668 **28**, 1693–702 (2012).

669 7. C. R. Diedrich, T. Rutledge, P. Maiello, T. M. Baranowski, A. G. White, H. J. Borish, P. Karell, F.
670 Hopkins, J. Brown, S. M. Fortune, J. L. Flynn, Z. Ambrose, P. L. Lin, SIV and Mycobacterium
671 tuberculosis synergy within the granuloma accelerates the reactivation pattern of latent
672 tuberculosis. *PLOS Pathog.* **16**, e1008413 (2020).

673 8. C. R. Diedrich, J. T. Mattila, E. Klein, C. Janssen, J. Phuah, T. J. Sturgeon, R. C. Montelaro, P. L.
674 Lin, J. A. L. Flynn, Reactivation of latent tuberculosis in cynomolgus macaques infected with SIV
675 is associated with early peripheral T cell depletion and not virus load. *PLoS One*. **5** (2010),
676 doi:10.1371/journal.pone.0009611.

677 9. H. Esmail, C. Riou, E. du Bruyn, R. P.-J. Lai, Y. X. R. Harley, G. Meintjes, K. A. Wilkinson, R. J.

678 Wilkinson, The Immune Response to Mycobacterium tuberculosis in HIV-1-Coinfected Persons.
679 *Annu. Rev. Immunol.* **36**, 603–638 (2018).
680 10. M. D. Tameris, M. Hatherill, B. S. Landry, T. J. Scriba, M. A. Snowden, S. Lockhart, J. E. Shea, J.
681 B. McClain, G. D. Hussey, W. A. Hanekom, H. Mahomed, H. McShane, MVA85A 020 Trial Study
682 Team, Safety and efficacy of MVA85A, a new tuberculosis vaccine, in infants previously
683 vaccinated with BCG: a randomised, placebo-controlled phase 2b trial. *Lancet (London, England)*.
684 **381**, 1021–8 (2013).
685 11. H. A. Fletcher, M. A. Snowden, B. Landry, W. Rida, I. Satti, S. A. Harris, M. Matsumiya, R.
686 Tanner, M. K. Oshea, V. Dheenadhayalan, L. Bogardus, L. Stockdale, L. Marsay, A. Chomka, R.
687 Harrington-Kandt, Z. R. Manjaly-Thomas, V. Naranbhai, E. Stylianou, F. Darboe, A. Penn-
688 Nicholson, E. Nemes, M. Hatheril, G. Hussey, H. Mahomed, M. Tameris, J. B. McClain, T. G.
689 Evans, W. A. Hanekom, T. J. Scriba, H. McShane, T-cell activation is an immune correlate of risk
690 in BCG vaccinated infants. *Nat. Commun.* **7** (2016), doi:10.1038/ncomms11290.
691 12. D. R. Tait, M. Hatherill, O. Van Der Meeren, A. M. Ginsberg, E. Van Brakel, B. Salaun, T. J.
692 Scriba, E. J. Akite, H. M. Ayles, A. Bollaerts, M.-A. Demoitié, A. Diacon, T. G. Evans, P. Gillard,
693 E. Hellström, J. C. Innes, M. Lempicki, M. Malahleha, N. Martinson, D. Mesia Vela, M. Muyoyeta,
694 V. Nduba, T. G. Pascal, M. Tameris, F. Thienemann, R. J. Wilkinson, F. Roman, Final Analysis
695 of a Trial of M72/AS01 E Vaccine to Prevent Tuberculosis . *N. Engl. J. Med.* **381**, 2429–2439
696 (2019).
697 13. O. Van Der Meeren, M. Hatherill, V. Nduba, R. J. Wilkinson, M. Muyoyeta, E. Van Brakel, H. M.
698 Ayles, G. Henostroza, F. Thienemann, T. J. Scriba, A. Diacon, G. L. Blatner, M.-A. Demoitié, M.
699 Tameris, M. Malahleha, J. C. Innes, E. Hellström, N. Martinson, T. Singh, E. J. Akite, A. Khatoon
700 Azam, A. Bollaerts, A. M. Ginsberg, T. G. Evans, P. Gillard, D. R. Tait, Phase 2b Controlled Trial
701 of M72/AS01E Vaccine to Prevent Tuberculosis. *N. Engl. J. Med.* **379**, 1621–1634 (2018).
702 14. E. Nemes, H. Geldenhuys, V. Rozot, K. T. Rutkowski, F. Ratangee, N. Bilek, S. Mabwe, L.

703 Makhethe, M. Erasmus, A. Toefy, H. Mulenga, W. A. Hanekom, S. G. Self, L.-G. Bekker, R. Ryall,
704 S. Gurunathan, C. A. DiazGranados, P. Andersen, I. Kromann, T. Evans, R. D. Ellis, B. Landry, D.
705 A. Hokey, R. Hopkins, A. M. Ginsberg, T. J. Scriba, M. Hatherill, C-040-404 Study Team,
706 Prevention of *M. tuberculosis* Infection with H4:IC31 Vaccine or BCG Revaccination. *N. Engl. J.*
707 *Med.* **379**, 138–149 (2018).
708 15. R. L. Anacker, W. Brehmer, W. R. Barclay, W. R. Leif, E. Ribi, J. H. Simmons, A. W. Smith,
709 Superiority of intravenously administered BCG and BCG cell walls in protecting rhesus monkeys
710 (Macaca mulatta) against airborne tuberculosis. *Z. Immunitatsforsch. Exp. Klin. Immunol.* **143**,
711 363–76 (1972).
712 16. W. R. Barclay, W. M. Busey, D. W. Dalgard, R. C. Good, B. W. Janicki, J. E. Kasik, E. Ribi, C. E.
713 Ulrich, E. Wolinsky, Protection of monkeys against airborne tuberculosis by aerosol vaccination
714 with bacillus Calmette-Guerin. *Am. Rev. Respir. Dis.* **107**, 351–8 (1973).
715 17. W. R. Barclay, R. L. Anacker, W. Brehmer, W. Leif, E. Ribi, Aerosol-Induced Tuberculosis in
716 Subhuman Primates and the Course of the Disease After Intravenous BCG Vaccination. *Infect.*
717 *Immun.* **2**, 574–82 (1970).
718 18. E. Ribi, R. L. Anacker, W. R. Barclay, W. Brehmer, S. C. Harris, W. R. Leif, J. Simmons, Efficacy
719 of mycobacterial cell walls as a vaccine against airborne tuberculosis in the Rhesus monkey. *J.*
720 *Infect. Dis.* **123**, 527–538 (1971).
721 19. S. Sharpe, A. White, C. Sarfas, L. Sibley, F. Gleeson, A. McIntyre, R. Basaraba, S. Clark, G. Hall,
722 E. Rayner, A. Williams, P. D. Marsh, M. Dennis, Alternative BCG delivery strategies improve
723 protection against Mycobacterium tuberculosis in non-human primates: Protection associated with
724 mycobacterial antigen-specific CD4 effector memory T-cell populations. *Tuberculosis (Edinb).*
725 **101**, 174–190 (2016).
726 20. P. A. Darrah, J. J. Zeppa, P. Maiello, J. A. Hackney, M. H. Wadsworth, T. K. Hughes, S. Pokkali,
727 P. A. Swanson, N. L. Grant, M. A. Rodgers, M. Kamath, C. M. Causgrove, D. J. Laddy, A. Bonavia,

728 D. Casimiro, P. L. Lin, E. Klein, A. G. White, C. A. Scanga, A. K. Shalek, M. Roederer, J. A. L.
729 Flynn, R. A. Seder, Prevention of tuberculosis in macaques after intravenous BCG immunization.
730 *Nature*. **577**, 95–102 (2020).
731 21. A. W. Chung, M. P. Kumar, K. B. Arnold, W. H. Yu, M. K. Schoen, L. J. Dunphy, T. J. Suscovich,
732 N. Frahm, C. Linde, A. E. Mahan, M. Hoffner, H. Streeck, M. E. Ackerman, M. J. McElrath, H.
733 Schuitemaker, M. G. Pau, L. R. Baden, J. H. Kim, N. L. Michael, D. H. Barouch, D. A.
734 Lauffenburger, G. Alter, Dissecting Polyclonal Vaccine-Induced Humoral Immunity against HIV
735 Using Systems Serology. *Cell*. **163**, 988–998 (2015).
736 22. D. Kaushal, T. W. Foreman, U. S. Gautam, X. Alvarez, T. Adekambi, J. Rangel-Moreno, N. A.
737 Golden, A. M. F. Johnson, B. L. Phillips, M. H. Ahsan, K. E. Russell-Lodrigue, L. A. Doyle, C. J.
738 Roy, P. J. Didier, J. L. Blanchard, J. Rengarajan, A. A. Lackner, S. A. Khader, S. Mehra, Mucosal
739 vaccination with attenuated Mycobacterium tuberculosis induces strong central memory responses
740 and protects against tuberculosis. *Nat. Commun.* **6** (2015), doi:10.1038/ncomms9533.
741 23. E. P. Brown, A. F. Licht, A.-S. Dugast, I. Choi, C. Bailey-Kellogg, G. Alter, M. E. Ackerman,
742 High-throughput, multiplexed IgG subclassing of antigen-specific antibodies from clinical samples.
743 *J. Immunol. Methods*. **386**, 117–23 (2012).
744 24. H. Yang, N. A. Kruh-Garcia, K. M. Dobos, Purified protein derivatives of tuberculin - past, present,
745 and future. *FEMS Immunol. Med. Microbiol.* **66** (2012), pp. 273–280.
746 25. A. K. Mishra, N. N. Driessen, B. J. Appelmelk, G. S. Besra, Lipoarabinomannan and related
747 glycoconjugates: structure, biogenesis and role in Mycobacterium tuberculosis physiology and
748 host-pathogen interaction. *FEMS Microbiol. Rev.* **35**, 1126–57 (2011).
749 26. Y. Yuan, D. D. Crane, R. M. Simpson, Y. Q. Zhu, M. J. Hickey, D. R. Sherman, C. E. Barry, The
750 16-kDa alpha-crystallin (Acr) protein of Mycobacterium tuberculosis is required for growth in
751 macrophages. *Proc. Natl. Acad. Sci. U. S. A.* **95**, 9578–83 (1998).
752 27. M. Esparza, B. Palomares, T. García, P. Espinosa, E. Zenteno, R. Mancilla, PstS-1, the 38-kDa

753 Mycobacterium tuberculosis glycoprotein, is an adhesin, which binds the macrophage mannose
754 receptor and promotes phagocytosis. *Scand. J. Immunol.* **81**, 46–55 (2015).
755 28. A. Ragas, L. Roussel, G. Puzo, M. Rivière, The Mycobacterium tuberculosis cell-surface
756 glycoprotein apa as a potential adhesin to colonize target cells via the innate immune system
757 pulmonary C-type lectin surfactant protein A. *J. Biol. Chem.* **282**, 5133–5142 (2007).
758 29. L. L. Lu, T. J. Suscovich, S. M. Fortune, G. Alter, Beyond binding: antibody effector functions in
759 infectious diseases. *Nat. Rev. Immunol.* **18**, 46–61 (2018).
760 30. P. J. Maglione, J. Xu, A. Casadevall, J. Chan, Fc gamma receptors regulate immune activation and
761 susceptibility during Mycobacterium tuberculosis infection. *J. Immunol.* **180**, 3329–38 (2008).
762 31. G. Alter, J. M. Malenfant, M. Altfeld, CD107a as a functional marker for the identification of
763 natural killer cell activity. *J. Immunol. Methods*. **294**, 15–22 (2004).
764 32. L. L. Lu, A. W. Chung, T. R. Rosebrock, M. Ghebremichael, W. H. Yu, P. S. Grace, M. K. Schoen,
765 F. Tafesse, C. Martin, V. Leung, A. E. Mahan, M. Sips, M. P. Kumar, J. Tedesco, H. Robinson, E.
766 Tkachenko, M. Draghi, K. J. Freedberg, H. Streeck, T. J. Suscovich, D. A. Lauffenburger, B. I.
767 Restrepo, C. Day, S. M. Fortune, G. Alter, A Functional Role for Antibodies in Tuberculosis. *Cell*.
768 **167**, 433-443.e14 (2016).
769 33. C. J. Martin, M. G. Booty, T. R. Rosebrock, C. Nunes-Alves, D. M. Desjardins, I. Keren, S. M.
770 Fortune, H. G. Remold, S. M. Behar, Efferocytosis is an innate antibacterial mechanism. *Cell Host*
771 *Microbe*. **12**, 289–300 (2012).
772 34. R. Roy Chowdhury, F. Vallania, Q. Yang, C. J. Lopez Angel, F. Darboe, A. Penn-Nicholson, V.
773 Rozot, E. Nemes, S. T. Malherbe, K. Ronacher, G. Walzl, W. Hanekom, M. M. Davis, J. Winter,
774 X. Chen, T. J. Scriba, P. Khatri, Y. Chien, A multi-cohort study of the immune factors associated
775 with M. tuberculosis infection outcomes. *Nature*. **560**, 644–648 (2018).
776 35. Y. Benjamini, Y. Hochberg, Controlling the False Discovery Rate: A Practical and Powerful
777 Approach to Multiple Testing. *J. R. Stat. Soc. Ser. B*. **57**, 289–300 (1995).

778 36. J. Friedman, T. Hastie, R. Tibshirani, Regularization Paths for Generalized Linear Models via
779 Coordinate Descent. *J. Stat. Softw.* **33**, 1–22 (2010).
780 37. F. Rohart, B. Gautier, A. Singh, K.-A. Lê Cao, mixOmics: An R package for ’omics feature
781 selection and multiple data integration. *PLoS Comput. Biol.* **13**, e1005752 (2017).
782 38. L. C. Lee, C.-Y. Liong, A. A. Jemain, Partial least squares-discriminant analysis (PLS-DA) for
783 classification of high-dimensional (HD) data: a review of contemporary practice strategies and
784 knowledge gaps. *Analyst*. **143**, 3526–3539 (2018).
785 39. B. Hamasur, M. Haile, A. Pawlowski, U. Schroder, G. Kallenius, S. B. Svenson, A mycobacterial
786 lipoarabinomannan specific monoclonal antibody and its F(ab’) fragment prolong survival of mice
787 infected with Mycobacterium tuberculosis. *Clin. Exp. Immunol.* **138**, 30–8 (2004).
788 40. R. Teitelbaum, A. Glatman-Freedman, B. Chen, J. B. Robbins, E. Unanue, A. Casadevall, B. R.
789 Bloom, □ Howard, A mAb recognizing a surface antigen of Mycobacterium tuberculosis enhances
790 host survival. *Microbiology*. **95**, 15688–15693 (1998).
791 41. K. Pethe, S. Alonso, F. Biet, G. Delogu, M. J. Brennan, C. Locht, F. D. Menozzi, The heparin-
792 binding haemagglutinin of M. tuberculosis is required for extrapulmonary dissemination. *Nature*.
793 **412**, 190–4 (2001).
794 42. S. Balu, R. Reljic, M. J. Lewis, R. J. Pleass, R. McIntosh, C. van Kooten, M. van Egmond, S.
795 Challacombe, J. M. Woof, J. Ivanyi, A novel human IgA monoclonal antibody protects against
796 tuberculosis. *J. Immunol.* **186**, 3113–9 (2011).
797 43. H. Li, X.-X. Wang, B. Wang, L. Fu, G. Liu, Y. Lu, M. Cao, H. Huang, B. Javid, Latently and
798 uninfected healthcare workers exposed to TB make protective antibodies against Mycobacterium
799 tuberculosis. *Proc. Natl. Acad. Sci. U. S. A.* **114**, 5023–5028 (2017).
800 44. E. Roy, E. Stavropoulos, J. Brennan, S. Coade, E. Grigorieva, B. Walker, B. Dagg, R. E. Tascon,
801 D. B. Lowrie, M. J. Colston, S. Jolles, Therapeutic efficacy of high-dose intravenous
802 immunoglobulin in Mycobacterium tuberculosis infection in mice. *Infect. Immun.* **73**, 6101–9

803 (2005).
804 45. A. Choudhary, D. Patel, W. Honnen, Z. Lai, R. S. Prattipati, R. B. Zheng, Y.-C. Hsueh, M. L.
805 Gennaro, A. Lardizabal, B. I. Restrepo, M. Garcia-Viveros, M. Joe, Y. Bai, K. Shen, K. Sahloul, J.
806 S. Spencer, D. Chatterjee, T. Broger, T. L. Lowary, A. Pinter, Characterization of the Antigenic
807 Heterogeneity of Lipoarabinomannan, the Major Surface Glycolipid of Mycobacterium
808 tuberculosis , and Complexity of Antibody Specificities toward This Antigen . *J. Immunol.* **200**,
809 3053–3066 (2018).
810 46. N. Andreu, A. Zelmer, T. Fletcher, P. T. Elkington, T. H. Ward, J. Ripoll, T. Parish, G. J. Bancroft,
811 U. Schaible, B. D. Robertson, S. Wiles, Optimisation of bioluminescent reporters for use with
812 mycobacteria. *PLoS One*. **5**, e10777 (2010).
813 47. J. M. Achkar, A. Casadevall, Antibody-Mediated Immunity against Tuberculosis: Implications for
814 Vaccine Development. *Cell Host Microbe*. **13**, 250–262 (2013).
815 48. R. E. Mebius, G. Kraal, Structure and function of the spleen. *Nat. Rev. Immunol.* **5** (2005), pp. 606–
816 616.
817 49. R. A. Mason, N. M. Tauraso, R. O. Spertzel, R. K. Ginn, Yellow fever vaccine: direct challenge of
818 monkeys given graded doses of 17D vaccine. *Appl. Microbiol.* **25**, 539–44 (1973).
819 50. H. Faden, J. F. Modlin, M. L. Thoms, A. M. McBean, M. B. Ferdon, P. L. Ogra, Comparative
820 evaluation of immunization with live attenuated and enhanced-potency inactivated trivalent
821 poliovirus vaccines in childhood: systemic and local immune responses. *J. Infect. Dis.* **162**, 1291–
822 7 (1990).
823 51. A. D. Jack, A. J. Hall, N. Maine, M. Mendy, H. C. Whittle, What Level of Hepatitis B Antibody Is
824 Protective? *J. Infect. Dis.* **179**, 489–492 (1999).
825 52. L. H. Lee, C. E. Frasch, L. A. Falk, D. L. Klein, C. D. Deal, Correlates of immunity for
826 pneumococcal conjugate vaccines. *Vaccine*. **21**, 2190–6 (2003).
827 53. I. Frazer, Correlating immunity with protection for HPV infection. *Int. J. Infect. Dis.* **11**, S10–S16

828 (2007).
829 54. S. A. Plotkin, Correlates of Protection Induced by Vaccination. *Clin. Vaccine Immunol.* **17**, 1055–
830 1065 (2010).
831 55. A. K. Wheatley, S. J. Kent, Prospects for antibody-based universal influenza vaccines in the context
832 of widespread pre-existing immunity. *Expert Rev. Vaccines*. **14**, 1227–1239 (2015).
833 56. M. R. Ehrenstein, C. A. Notley, The importance of natural IgM: scavenger, protector and regulator.
834 *Nat. Rev. Immunol.* **10**, 778–86 (2010).
835 57. V. B. Klimovich, IgM and its receptors: Structural and functional aspects. *Biochem.* **76** (2011), pp.
836 534–549.
837 58. A. Meryk, L. Pangrazzi, M. Hagen, F. Hatzmann, B. Jenewein, B. Jakic, N. Hermann-Kleiter, G.
838 Baier, J. Jylhävä, M. Hurme, K. Trieb, B. Grubeck-Loebenstein, Fcμ receptor as a Costimulatory
839 Molecule for T Cells. *Cell Rep.* **26**, 2681-2691.e5 (2019).
840 59. T. Broger, B. Sossen, E. du Toit, A. D. Kerkhoff, C. Schutz, E. Ivanova Reipold, A. Ward, D. A.
841 Barr, A. Macé, A. Trollip, R. Burton, S. Ongarello, A. Pinter, T. L. Lowary, C. Boehme, M. P.
842 Nicol, G. Meintjes, C. M. Denkinger, Novel lipoarabinomannan point-of-care tuberculosis test for
843 people with HIV: a diagnostic accuracy study. *Lancet Infect. Dis.* **19**, 852–861 (2019).
844 60. G. B. Sigal, A. Pinter, T. L. Lowary, M. Kawasaki, A. Li, A. Mathew, M. Tsionsky, R. B. Zheng,
845 T. Plisova, K. Shen, K. Katsuragi, A. Choudhary, W. J. Honnen, P. Nahid, C. M. Denkinger, T.
846 Broger, A novel sensitive immunoassay targeting the 5-methylthio-D-xylofuranose–
847 lipoarabinomannan epitope meets the WHO's performance target for tuberculosis diagnosis. *J.*
848 *Clin. Microbiol.* **56** (2018), doi:10.1128/JCM.01338-18.
849 61. T. Broger, M. P. Nicol, G. B. Sigal, E. Gotuzzo, A. J. Zimmer, S. Surtie, T. Caceres-Nakiche, A.
850 Mantsoki, E. I. Reipold, R. Székely, M. Tsionsky, J. van Heerden, T. Plisova, K. Chikamatsu, T.
851 L. Lowary, A. Pinter, S. Mitarai, E. Moreau, S. G. Schumacher, C. M. Denkinger, Diagnostic
852 accuracy of 3 urine lipoarabinomannan tuberculosis assays in HIV-negative outpatients. *J. Clin.*

853 *Invest.* **130** (2020), doi:10.1172/jci140461.

854 62. K. Dijkman, C. C. Sombroek, R. A. W. Vervenne, S. O. Hofman, C. Boot, E. J. Remarque, C. H.
855 M. Kocken, T. H. M. Ottenhoff, I. Kondova, M. A. Khayum, K. G. Haanstra, M. P. M. Vierboom,
856 F. A. W. Verreck, Prevention of tuberculosis infection and disease by local BCG in repeatedly
857 exposed rhesus macaques. *Nat. Med.* **25**, 255–262 (2019).

858 63. V. Balasubramanian, E. H. Wiegeshaus, B. T. Taylor, D. W. Smith, Pathogenesis of tuberculosis:
859 pathway to apical localization. *Tuber. Lung Dis.* **75** (1994), pp. 168–178.

860 64. S. R. Allie, J. E. Bradley, U. Mudunuru, M. D. Schultz, B. A. Graf, F. E. Lund, T. D. Randall, The
861 establishment of resident memory B cells in the lung requires local antigen encounter. *Nat.*
862 *Immunol.* **20**, 97–108 (2019).

863 65. T. Onodera, Y. Takahashi, Y. Yokoi, M. Ato, Y. Kodama, S. Hachimura, T. Kurosaki, K.
864 Kobayashi, Memory B cells in the lung participate in protective humoral immune responses to
865 pulmonary influenza virus reinfection. *Proc. Natl. Acad. Sci. U. S. A.* **109**, 2485–2490 (2012).

866 66. S. A. Schlottmann, N. Jain, N. Chirmule, M. T. Esser, A novel chemistry for conjugating
867 pneumococcal polysaccharides to Luminex microspheres. *J. Immunol. Methods*. **309**, 75–85
868 (2006).

869 67. E. van Woudenbergh, E. B. Irvine, L. Davies, M. de Kock, W. A. Hanekom, C. L. Day, S. Fortune,
870 G. Alter, HIV Is Associated with Modified Humoral Immune Responses in the Setting of HIV/TB
871 Coinfection. *mSphere*. **5** (2020), doi:10.1128/mSphere.00104-20.

872 68. E. P. Brown, K. G. Dowell, A. W. Boesch, E. Normandin, A. E. Mahan, T. Chu, D. H. Barouch, C.
873 Bailey-Kellogg, G. Alter, M. E. Ackerman, Multiplexed Fc array for evaluation of antigen-specific
874 antibody effector profiles. *J. Immunol. Methods*. **443**, 33–44 (2017).

875 69. M. E. Ackerman, B. Moldt, R. T. Wyatt, A. S. Dugast, E. McAndrew, S. Tsoukas, S. Jost, C. T.
876 Berger, G. Sciaranghella, Q. Liu, D. J. Irvine, D. R. Burton, G. Alter, A robust, high-throughput
877 assay to determine the phagocytic activity of clinical antibody samples. *J. Immunol. Methods*. **366**,

878 8–19 (2011).
879 70. C. B. Karsten, N. Mehta, S. A. Shin, T. J. Diefenbach, M. D. Slein, W. Karpinski, E. B. Irvine, T.
880 Broge, T. J. Suscovich, G. Alter, A versatile high-throughput assay to characterize antibody-
881 mediated neutrophil phagocytosis. *J. Immunol. Methods*. **471**, 46–56 (2019).
882 71. F. Bunea, Y. She, H. Ombao, A. Gongvatana, K. Devlin, R. Cohen, Penalized least squares
883 regression methods and applications to neuroimaging. *Neuroimage*. **55**, 1519–1527 (2011).
884
885
886
887
888
889
890
891
892
893
894
895
896
897
898
899
900
901
902

903 **Acknowledgements**

904 We thank the Vaccine research center at the National Institutes of Health for providing the rhesus macaque
905 plasma and BAL samples from the BCG route vaccination study. We thank the Tulane National Primate
906 Research Center for providing the rhesus macaque plasma samples from the attenuated *Mtb* (*Mtb-ΔsigH*)
907 vaccination study. We thank the Harvard Medical School, Laboratory for Systems Pharmacology for
908 allowing the use of their automated microscope.

909

910 **Funding**

911 Ragon Institute of MGH, MIT, and Harvard and the SAMANA Kay MGH Research Scholar Program.
912 Bill and Melinda Gates Foundation: OPP1156795.
913 Defense Advanced Research Projects Agency: W911NF-19-2-0017.
914 National Institutes of Health: U54CA225088, U2CCA233262, U2CCA233280, AI150171-01, and
915 Contract No. 75N93019C00071.

916

917 **Author Contributions**

918 E.B.I. – Conceptualization, Methodology, Software, Validation, Formal Analysis, Investigation, Data
919 Curation, Writing Original Draft, Review and Editing, Visualization, Funding Acquisition; A.O. –
920 Validation, Investigation, Review and Editing; P.A.D. – Conceptualization, Resources, Data Curation,
921 Review and Editing; S.S. – Investigation, Review and Editing; A.C. – Methodology, Resources, Review
922 and Editing; W.L. – Methodology, Review and Editing; W.H. – Validation, Investigation, Resources; S.M.
923 – Conceptualization, Methodology, Resources, Review and Editing; D.K. – Conceptualization,
924 Methodology, Resources, Data Curation, Review and Editing; H.P.G – Investigation, Resources, Data
925 Curation; J.L.F. – Conceptualization, Methodology, Resources, Review and Editing, Supervision; M.R. –
926 Conceptualization, Resources, Review and Editing, Supervision; R.A.S. – Conceptualization,
927 Methodology, Resources, Review and Editing, Supervision; A.P. – Conceptualization, Methodology,

928 Resources, Review and Editing, Supervision; S.F. – Conceptualization, Methodology, Resources, Review
929 and Editing, Supervision, Project Administration, Funding Acquisition; G.A. – Conceptualization,
930 Methodology, Resources, Review and Editing, Supervision, Project Administration, Funding Acquisition.
931

932 **Competing Interests**

933 Galit Alter is a founder of SeromYx Systems, Inc.
934

935 **Data and materials availability**

936 All data associated with this study are available in the main text or in the supplementary materials. Any
937 additional materials data, and code will be made available to members of the scientific community in a
938 timely fashion following a reasonable request.
939

940 **List of Supplementary Materials**

941 Figure S1: Antigen-specific FcγR binding capacity of plasma and BAL antibodies
942 Figure S2: Plasma IgG1 and IgA titers from the attenuated *Mtb* (*Mtb-ΔsigH*) vaccination cohort
943 Data S1: Data_SystemsSerology
944 Code S1: Code_LASSO_PLSDA
945
946
947
948
949
950
951
952

953 **FIGURES**

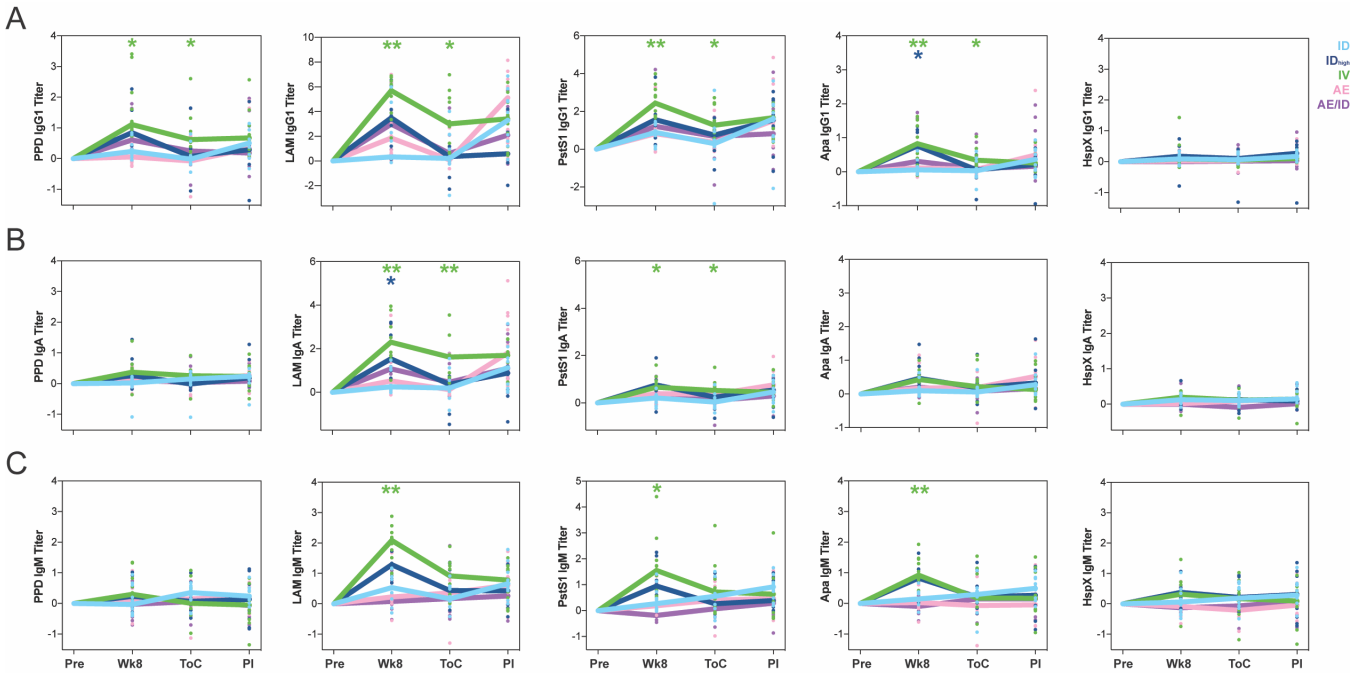

954

955 **Figure 1: IV BCG immunized primates exhibit higher and more durable plasma antibody titers.**
956 Fold change in (**A**) IgG1, (**B**) IgA, and (**C**) IgM titers present in the plasma of each rhesus macaque
957 following BCG vaccination were determined via Luminex. Fold changes were calculated as fold change
958 in Luminex median fluorescence intensity (MFI) over the pre-vaccination level for each primate. A base-
959 2 log scale is used for the y-axis. Timepoints: pre-vaccination (Pre), week 8 post-BCG vaccination (Wk8),
960 time of challenge at week 24 post-BCG vaccination (ToC), post-infection at week 28 post-BCG
961 vaccination (PI). Groups: standard intradermal BCG (light blue), high intradermal BCG (dark blue),
962 intravenous BCG (green), aerosol BCG (pink), aerosol + intradermal BCG (purple). Each dot represents
963 a single animal at the respective timepoint. The lines represent group medians over time. Kruskal-Wallis
964 with Dunn's multiple-comparison tests were performed on the fold change values at each timepoint,
965 comparing each vaccination group to the standard intradermal BCG group. Adjusted p-values are as
966 follows: *, $p < 0.05$; **, $p < 0.01$; ***, $p < 0.001$; ****, $p < 0.0001$.

967

968

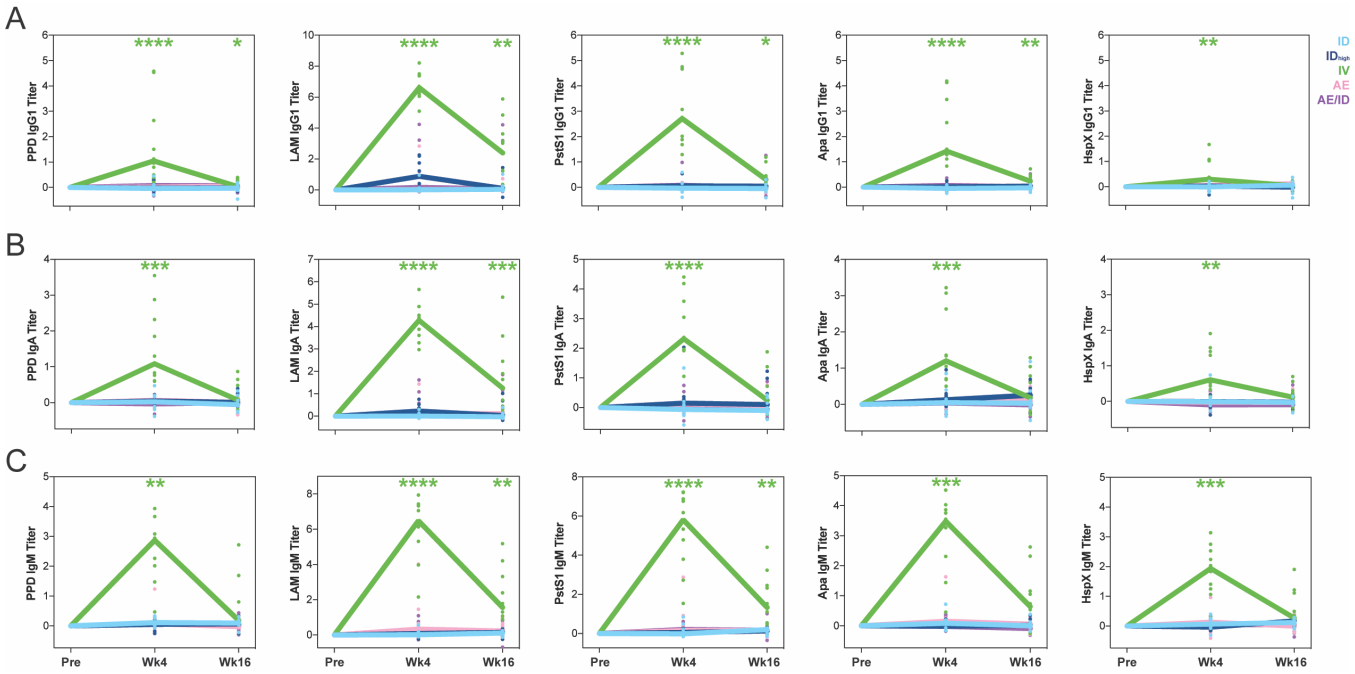

Figure 2: IV BCG vaccination uniquely elicits a robust lung-compartmentalized antibody response. Fold change in (**A**) IgG1, (**B**) IgA, and (**C**) IgM titers present in the BAL of each rhesus macaque following BCG vaccination were determined via Luminex. Fold changes were calculated as fold change in Luminex MFI over the pre-vaccination level for each primate. A base-2 log scale is used for the y-axis. Timepoints: pre-vaccination (Pre), week 4 post-BCG vaccination (Wk4), week 16 post-BCG vaccination (Wk16). Groups: standard intradermal BCG (light blue), high intradermal BCG (dark blue), intravenous BCG (green), aerosol BCG (pink), aerosol + intradermal BCG (purple). Each dot represents a single animal at the respective timepoint. The lines represent group medians over time. Kruskal-Wallis with Dunn's multiple-comparison tests were performed on the fold change values at each timepoint, comparing each vaccination group to the standard intradermal BCG group. Adjusted p-values are as follows: *, $p < 0.05$; **, $p < 0.01$; ***, $p < 0.001$; ****, $p < 0.0001$.

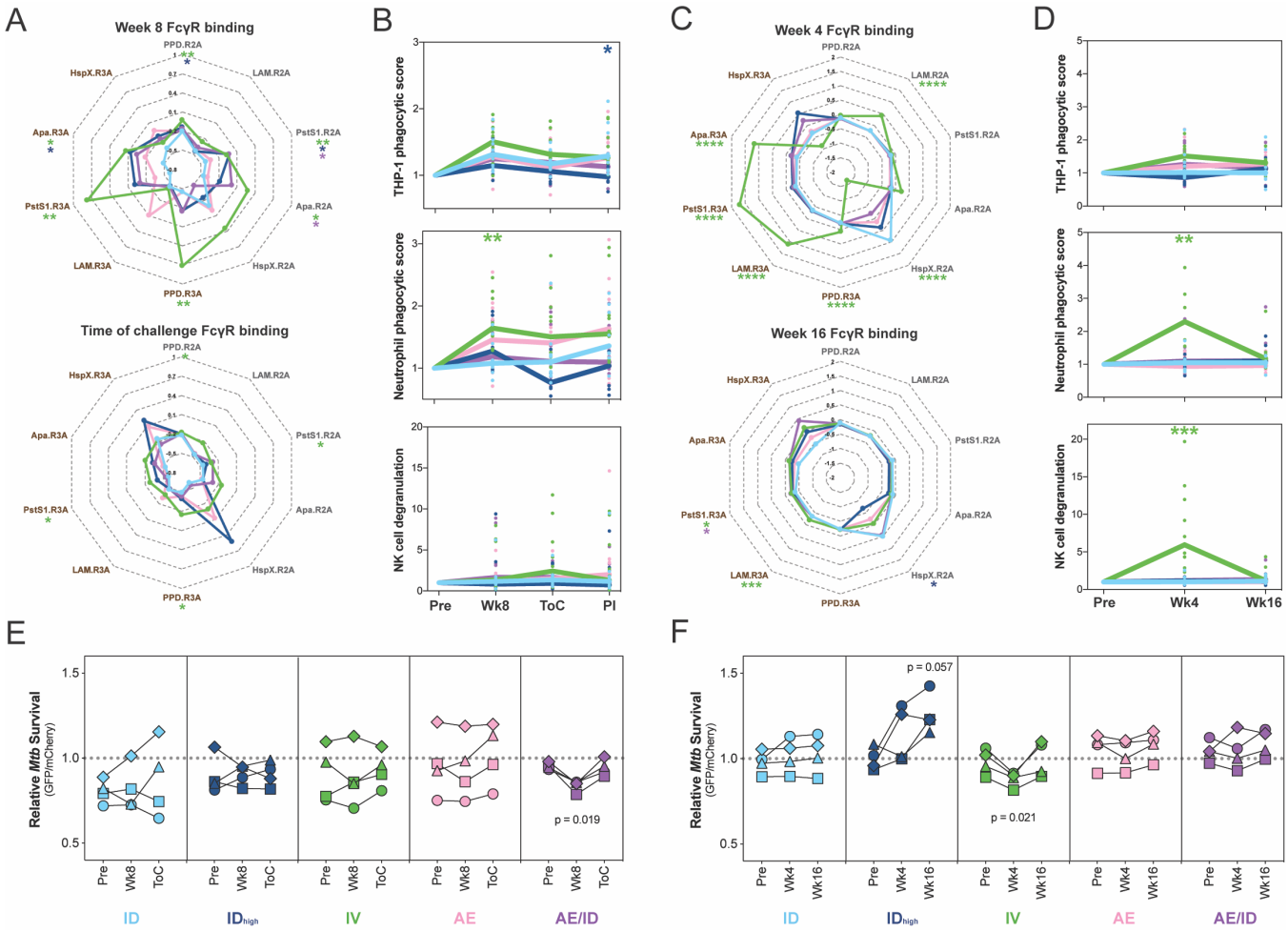

Figure 3: Antibodies from IV BCG vaccinated primates drive innate immune activation. (**A and C**) Radar plots of fold change in (**A**) plasma and (**C**) BAL antibody FcγR binding activity of each group post-BCG vaccination. Fold changes were calculated as fold change in Luminex MFI over the pre-vaccination level for each primate. Median z-score of each group is plotted for a given feature. (**B and D**) Fold change in (**B**) plasma and (**D**) BAL antibody-dependent cellular phagocytosis by THP-1 cells (top), antibody-dependent neutrophil phagocytosis by primary human neutrophils (middle), antibody-dependent primary human NK cell degranulation determined by % of cells CD107a positive (bottom). Fold changes were calculated as fold change over the pre-vaccination level for each primate. Each dot represents a single animal at the respective timepoint. The lines represent group medians over time. (**E and F**) *in vitro* macrophage *Mtb* survival assay using pooled (**E**) plasma and (**F**) BAL from each vaccination group at each timepoint. y-axis shows live (GFP) / total (mCherry) *Mtb* burden in human monocyte-derived

macrophages. Lower on the y-axis indicates increased intracellular *Mtb* killing in macrophages. Each set of connected dots indicates the activity of pools from different timepoints run across the same healthy human macrophage donor; 4 donors were run in total. Plasma timepoints: pre-vaccination (Pre), week 8 post-BCG vaccination (Wk8), and time of challenge at week 24 post-BCG vaccination (ToC). BAL timepoints: pre-vaccination (Pre), week 4 post-BCG vaccination (Wk4), week 16 post-BCG vaccination (Wk16). Groups: standard intradermal BCG (light blue), high intradermal BCG (dark blue), intravenous BCG (green), aerosol BCG (pink), aerosol + intradermal BCG (purple). (**A – D**) Kruskal-Wallis with Dunn's multiple-comparison test was performed on the fold change values at each timepoint, comparing each vaccination group to the standard intradermal BCG group. (**E and F**) Repeated measures ANOVA with Dunnett's multiple comparisons test was performed for each vaccination group, comparing pre-vaccination restrictive activity with that of each post-vaccination timepoint. Adjusted p-values are as follows: *, $p < 0.05$; **, $p < 0.01$; ***, $p < 0.001$; ****, $p < 0.0001$.

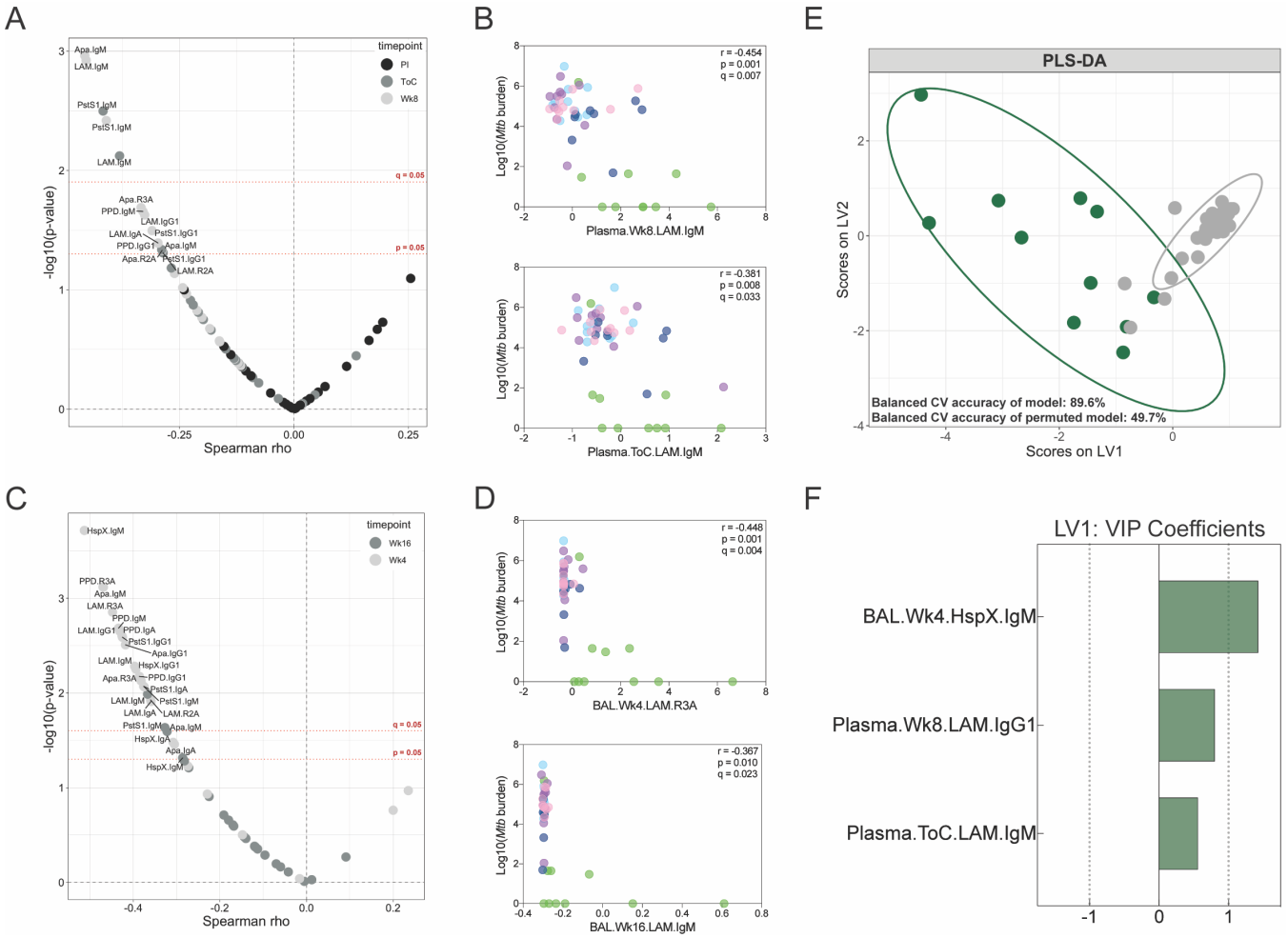

Figure 4: Numerous BCG-induced antibody features are associated with reduced *Mtb* burden. (**A and C**) Spearman correlations between base-10 log(*Mtb* burden) at necropsy and each (**A**) plasma and (**C**) BAL antibody measurement post-vaccination were computed. The x-axis indicates the spearman rho value associated with a given antibody feature. The y-axis indicates the negative base-10 log of the p-value associated with a given antibody feature. Antibody features are colored by their timepoint. (**A**) Plasma colors: week 8 post-BCG vaccination (light grey), time of challenge at week 24 post-BCG vaccination (dark grey), post-infection at week 28 post-BCG vaccination (black). (**C**) BAL colors: week 4 post-BCG vaccination (light grey), week 16 post-BCG vaccination (dark grey). (**B and D**) Spearman correlations between base-10 log(*Mtb* burden) at necropsy and select (**B**) plasma and (**D**) BAL antibody measurements. Points are colored by vaccination group: standard intradermal BCG (light blue), high intradermal BCG (dark blue), intravenous BCG (green), aerosol BCG (pink), aerosol + intradermal BCG (purple). Fold

1034 change antibody measurements were subjected to a z-score transformation prior to correlation analyses.
1035 Adjusted p-values (q-values) computed by the Benjamini-Hochberg procedure. (**E and F**) PLS-DA model
1036 fit using the antibody features selected by LASSO regularization. (**E**) Graph of the first two latent variables
1037 (LVs) of the model. Protected primates (green) had an *Mtb* burden < 1000 at necropsy. Susceptible
1038 primates (grey) had an *Mtb* burden > 1000 at necropsy. Ellipses show 95% confidence intervals. Balanced
1039 cross-validation (CV) accuracy of the model and permuted model are indicated. Accuracy of model is
1040 significantly higher than that of the permuted model (Mann-Whitney U test, $p < 2.2e^{-16}$). (**F**) Variable
1041 importance in the projection (VIP) coefficients on LV1 for each model feature, indicating the extent to
1042 which each feature contributes to separation along LV1.
1043
1044
1045
1046
1047
1048
1049
1050
1051
1052
1053
1054
1055
1056
1057
1058

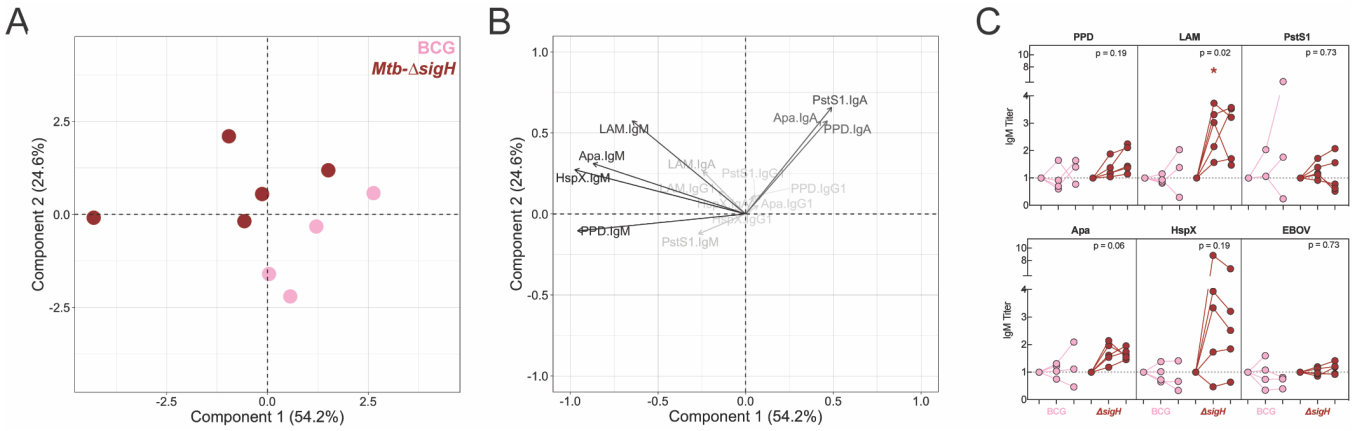

Figure 5: Protective vaccination with attenuated *Mtb* (*Mtb-ΔsigH*) is associated with increased plasma IgM titers. (**A and B**) Principal component analysis using fold change IgG1, IgA, and IgM titers measured at week 7 post-vaccination in an attenuated *Mtb* rhesus macaque vaccination cohort. Fold changes were calculated as fold change in Luminex MFI over the pre-vaccination level for each primate. Fold change antibody measurements were subjected to a z-score transformation prior to principal component analysis. (**A**) Score plot. Aerosol *Mtb-ΔsigH* vaccination group (red), aerosol BCG vaccination group (pink). (**B**) Loading plot. Relative contribution of variables to the components are indicated by a color gradient. Light grey variables contribute least, black variables contribute most. (**C**) Fold change in IgM titer present in the plasma of each rhesus macaque following vaccination determined via Luminex. Fold changes were calculated as fold change in Luminex MFI over the pre-vaccination level for each primate. Each dot represents a single animal at the respective timepoint. Timepoints: pre-vaccination (left), week 7 post-vaccination (middle), week 15 post-vaccination at necropsy (right). *Mtb* challenge was performed week 8 post-vaccination. Mann-Whitney U test was performed on the fold change values at each timepoint, comparing aerosol *Mtb-ΔsigH* to the aerosol BCG group. p-values are as follows: *, $p < 0.05$; **, $p < 0.01$; ***, $p < 0.001$; ****, $p < 0.0001$.

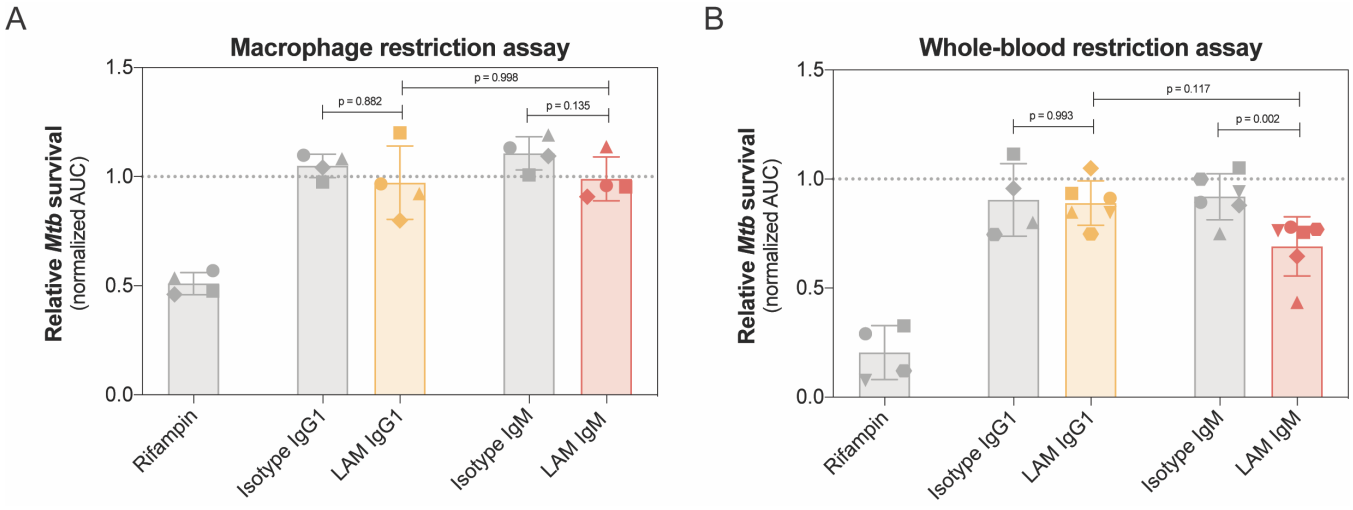

Figure 6: LAM IgM monoclonal antibody drives superior *Mtb* restriction in human whole-blood. (**A**) Macrophage restriction assay. Each antibody was added (final concentration 50ug/mL) to human monocyte-derived macrophages infected with a luminescent *Mtb* reporter strain (*Mtb-276*). Growth curves in the presence of each antibody treatment were generated by taking luminescence readings every 24 hours up to 120 hours. Y-axis is the area under the *Mtb* growth curve normalized by the no antibody condition of each donor. Each dot is the triplicate average from 1 donor. (**B**) Whole-blood restriction assay. Each antibody (final concentration 25ug/mL) was tested for their ability to drive *Mtb* restriction in the context of fresh human whole-blood using *Mtb-276*. Y-axis is the area under the *Mtb* growth curve, normalized by the no antibody condition. Growth curves were generated by taking luminescence readings every 24 hours up to 120 hours. Each dot is the triplicate average from 1 donor. Repeated measures ANOVA with Sidak's multiple comparisons test.